Hindawi
Complexity
Volume 2019, Article ID 2739212, 22 pages
https://doi.org/10.1155/2019/2739212

Research Article

Analysis on the Time-Varying Fragility of Offshore Concrete Bridge

Yan Liang,[1] Jia-lei Yan,[1] Jun-lei Wang ,[2] Peng Zhang ,[3] and Bao-jie He[4]

[1]*College of Civil Engineering, Zhengzhou University, Zhengzhou, China*
[2]*School of Chemical Engineering and Energy, Zhengzhou University, Zhengzhou, China*
[3]*School of Water Conservancy and Environment, Zhengzhou University, Zhengzhou, China*
[4]*Faculty of Built Environment, University of New South Wales, Sydney, NSW 2052, Australia*

Correspondence should be addressed to Jun-lei Wang; just4pipi@126.com

Received 21 November 2018; Revised 5 January 2019; Accepted 9 January 2019; Published 20 January 2019

Academic Editor: Guang Li

For offshore bridges, the most prominent problem in the whole life cycle is that it is in an earthquake prone zone and an offshore corrosion environment at the same time. A nonlinear dynamic analysis model is set up for an offshore multispan and continuous rigid frame bridge based on the OpenSEES platform. The fragility surface of the bridge pier, bearing, bridge platform, and system are established by selecting a reasonable damage constitutive model of the material durability and a damage index analysis that studies the damage of the bridge durability to time-varying seismic fragility of bridge components and the system of the whole life cycle in offshore environment. The results show that the durability damage will lead to a constant decline in seismic capacity of the pier and an increase of the seismic demand under earthquake action as well as the probability to reach the ultimate failure state; compared to high piers, a low pier is more vulnerable to the offshore corrosion environment; the seismic fragility of bridge platform is higher than that of simply bearing; and the influence of offshore corrosion on environment is relatively large. With the prolongation of service period, the effect of durability damage on the seismic fragility of bridge system cannot be ignored in the coastal environment and it is necessary to make a reasonable evaluation on the seismic fragility of bridge structure during the whole life period.

1. Introduction

So far, the offshore and cross sea bridges have been widely built around the world, such as the Ming Shi channel bridge in Japan, the Waal bridge in Netherland, and the Oakland Harbour Bridge in New Zealand. With a coastline of 18,000 km, China also has carried out the construction of offshore and cross sea bridges so as to promote the economic development of offshore areas, to meet the needs of offshore resources exploration and to maintain maritime sovereignty [1, 2]. Some of them have been completed such as the Hangzhou Bay Bridge built in 2008 and the Hong Kong Zhuhai Macao Bridge in 2016. But the consequent problem is the corrosion of concrete structures under the offshore environment. For the Offshore Bridge, the special geographical environment will seriously corrode the bridge structure material and make its mechanical properties degenerate, and the most prominent problem is that many bridges are in both the offshore corrosion environment and the earthquake multiple zones. The existing studies [3] show that as the service time of the bridge extends, the concrete carbonization and chloride ion erosion effect will cause durability damage to the bridge structure and then lead to degradation of the seismic performance.

Seismic fragility analysis is one of the main methods to evaluate seismic performance of the offshore bridges in the whole life cycle. Scholars at home and abroad have made a lot of research achievements. Considering the degradation effect of chloride ion erosion on the properties of reinforcing steel bars and by analyzing the seismic fragility of a two-span bridge, Choe and others [10] conclude that the corrosion of reinforcing steel bars will have a certain effect on the seismic performance of concrete bridges. A new intensity measure of earthquakes for probabilistic seismic analysis is presented

for skewed highway bridges by Bayat [11, 12]. Andre et al. [13] concerns the development of a new structural robustness definition, and structural robustness and structural fragility indices. Salimi and Yazdani [14] have studied that the reliability-based analysis of nonlinear structures using the analytical fragility curves are excited by random earthquake loads. A hybrid fiber reinforced polymer/reinforced concrete bridge was designed and constructed in Texas by Ziehl et al. [15], which was unique in several respects. In addition, the bid process and results of intermittent live load evaluations that have been conducted over a period of approximately 2 years are presented. The incremental nonlinear dynamic analysis is used to evaluate the seismic performance of steel moment frame structures by Khorami et al. [16]. Ghosh and Padgett [17] proposed a two-model of seismic fragility parameters to discuss the effect of chloride ion erosion on the time variation of bridge and the influence of the deterioration of component performance on seismic fragility of bridges subjected to chloride attack. Jeon et al. [18] suggest that the earthquake incidence angle more significantly affects the seismic demand and fragilities of the integral bridge platform bridge than the skewed bridge platform bridge. Waseem et al. [19] present seismic vulnerability assessment of three real case simply bearing multispan reinforced concrete bridges commonly found in northern Pakistan, having one, two, and three bents with circular piers. Simon et al. [20] take steel corrosion and protective concrete cracking as variables to establish the no damage model, steel corrosion model, protective concrete failure model and reinforcement corrosion, and protective concrete failure model of a single pier bridge based on the *OpenSEES* program to analyze the effect of reinforcement corrosion and protective concrete failure on the fragility of concrete bridge. Alipour et al. [21] study the life-cycle performance and cost of reinforced concrete highway bridges subjected to earthquake ground motions when they are continuously exposed to the attack of chloride ions and provide a multihazard framework that will achieve more realistic performance and cost estimates. Cui et al. [22] present an improved reinforced concrete reinforcing steel bar deterioration model that incorporates pitting corrosion and considers the change in after-cracking corrosion rate to assess the time-dependent seismic fragility of RC bridge substructures in marine environments. The calculated time-dependent fragility curves indicate that there is a nonlinear accelerated growth of RC column vulnerability along the service life of highway bridges, especially after twenty-five years' exposure to chlorides. Deng et al. [23] reveal that the corrosion-induced deterioration of strain penetration and rebar yield strength significantly increase the seismic fragility of the corroded MSSS bridge.

To sum up, with regard to the effect of steel corrosion on seismic fragility of bridges, relevant research results have been obtained at home and abroad. However, the traditional research often ignores the problem of seismic performance degradation of bridge structures during the whole life cycle. As a result, some bridges cannot reach the design service life and need to be repaired and strengthened to maintain their normal function, thus leading to a lot of economic losses.

2. The Establishment of Nonlinear Finite Element Model Based on *OpenSEES*

The *OpenSEES* analysis platform can be used for structural modal analysis, section analysis, static linear elastic analysis, dynamic nonlinear analysis, and the sensitivity and reliability analysis of structural systems in earthquake [22–24]. In this paper, a finite element model of bridge is established based on *OpenSEES* platform.

In this paper, the bridge is a 6 span ($6 \times 60\,\text{m} = 360\,\text{m}$) prestressed concrete rigid frame continuous girder bridge in which $2^{\#}$ and $3^{\#}$ piers are fixed piers, while $1^{\#}$, $4^{\#}$, and $5^{\#}$ piers are simply-bearing ones. The seismic fortification intensity in the area where the bridge is located is 7 degrees, and the earthquake is divided into the first group and the site soil is the class II site. The facade arrangement is shown in Figure 1(a). According to the soil category of the bridge site, seismic waves are selected from the *PEER* ground motion database. Considering the uncertainty of the earthquake and structural damage indexes, the seismic fragility analysis is established and the nonlinear finite element modeling of this example is completed.

The deck is one box single chamber box section, and the Elastic Beam Column unit, the fiber element based on the flexibility method-nonlinear Beam Column unit, the nonlinear connection unit, and zero-length element which are used to simulate the deck, the nonlinear characteristics of the pier, the bridge platform ball bearing, and bridge platform separately. In addition, the area of deck is $A = 9.5\,\text{m}^2$, Young's modulus of elasticity of deck concrete ($C50$) is $E = 3.45 \times 10^4$ MPa, poisson ratio is $\mu = 0.2$, torsional inertia moment of deck section is $J = 25.8\,\text{m}^4$, and bending moment of inertia of cross section in z-axis and y-axis direction are $I_z = 14.3\,\text{m}^4$ and $I_y = 82.4\,\text{m}^4$, as shown in Figure 1(b); the section of pier is shown in Figure 1(c); in the Figure 1(d), 1 is lower plate, 2 is spherical F4 Plate, 3 is sealed skirt, 4 is mid-seat plate, 5 is planar F4 plate, 6 is upper slide plate, and 7 is upper seat plate and bridge abutment model as shown in Figure 1(e).

3. Model of Material

3.1. Constitutive Relation and Mechanical Properties of Concrete

3.1.1. Constitutive Relation of Concrete. The ductility of the pier is mainly reflected by plastic rotation capacity in the plastic hinge of the pier. The concrete in the core area has a particularly higher ultimate compressive strain than the unconstrained concrete before the failure of the compression zone, which can ensure the ductility required by the structure [25–27]. Therefore, it is necessary to separate the protective concrete from the core concrete. Unconstrained and constrained concrete materials are simulated by using the Concrete 01 model as shown in Figure 2, and the stress-strain relationship curve is shown in Figure 3. And the related parameters for the calculating of stress and strain are shown

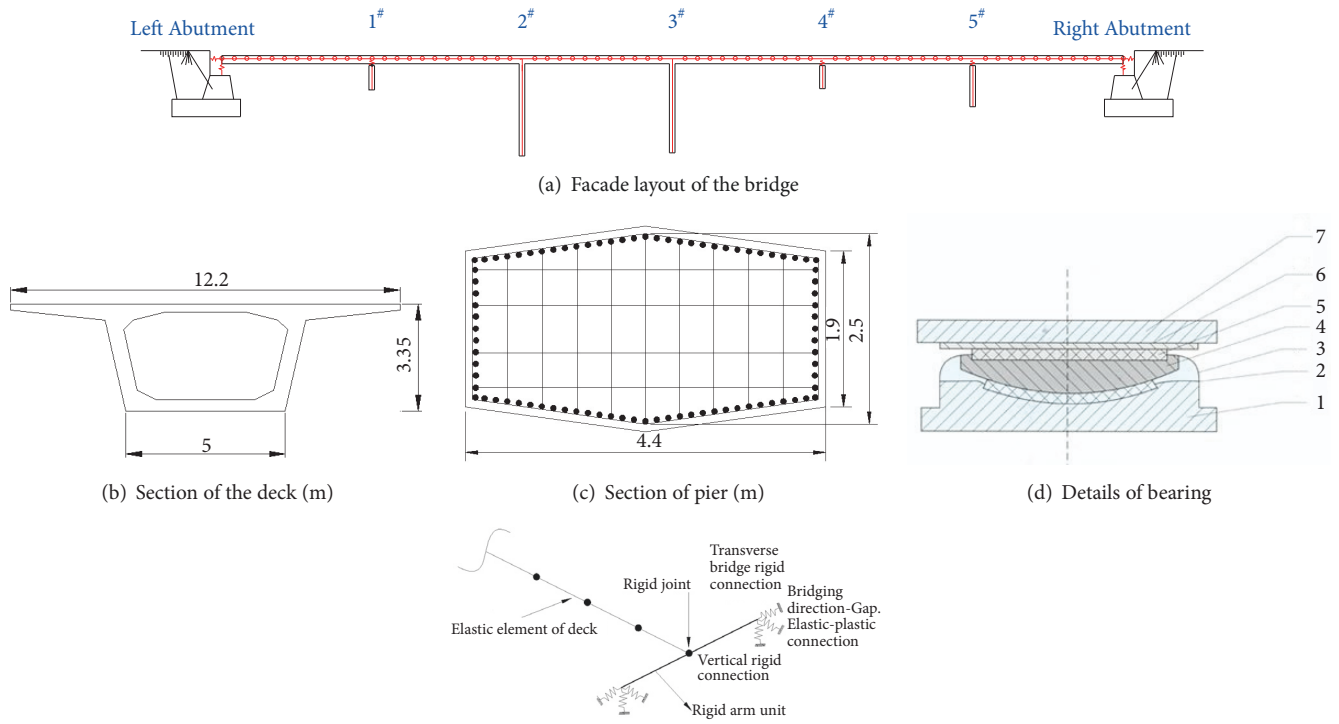

(a) Facade layout of the bridge

(b) Section of the deck (m)

(c) Section of pier (m)

(d) Details of bearing

(e) Abutment model

Figure 1: General arrangement diagram for bridge.

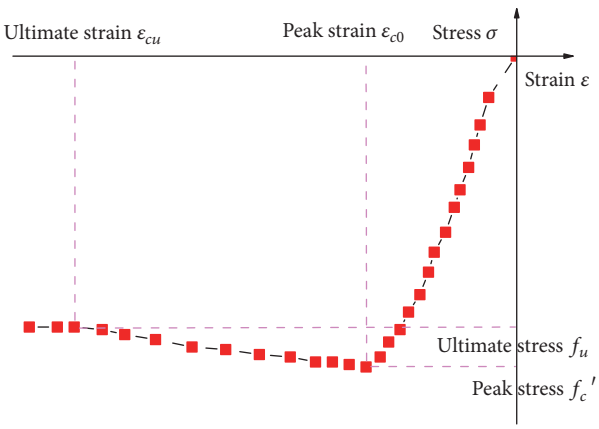

Figure 2: Constitutive relation of concrete 01.

in

$$f_{cc} = (1 + 1.79\lambda_V) f_{c0} \quad (1)$$

$$\varepsilon_{cc} = (1 + 3.5\lambda_V) \varepsilon_{c0} \quad (2)$$

$$\lambda_V = \frac{d \cdot f_{yh}}{f_{c0}} \quad (3)$$

$$\varepsilon_{cu} = 0.004 + \frac{1.4\rho_s \cdot f_{yh} \cdot \varepsilon_{su}}{f'_{cc}} \quad (4)$$

In the formulas, f_{cc} is the axial compressive strength of concrete in core area and f'_{cc} is the axial compressive strength of unconstrained concrete. f_{c0} is axial compressive strength of concrete, ε_{cc} is axial compressive strain of concrete in core area, and ε_{c0} is axial compressive strain of concrete, which is generally -0.002, λ_V is stirrup eigenvalue, d is volume radio of reinforcement, which is calculated by the lipid of stirrups, and f_{yh} is yield strength of stirrups. ε_{cu} is ultimate compressive strain of confined concrete, which is generally -0.004, ε_{su} is strain of stirrups under maximum tensile stress, which is generally 0.09, and ρ_s is volume reinforcement ratio of stirrups.

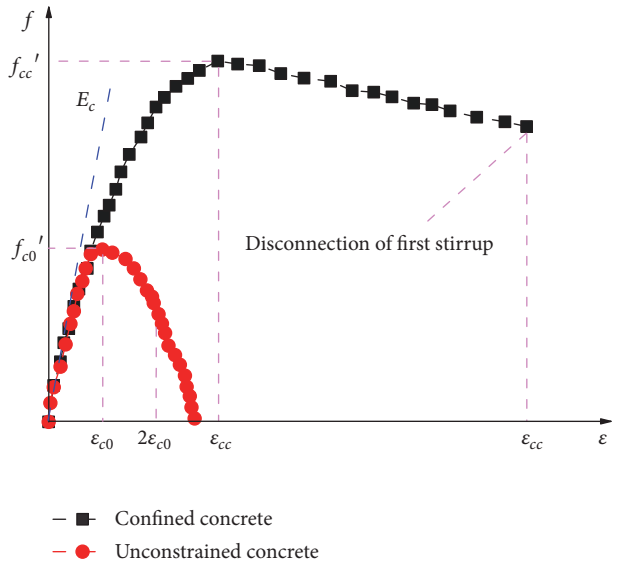

Figure 3: Stress-strain relationship.

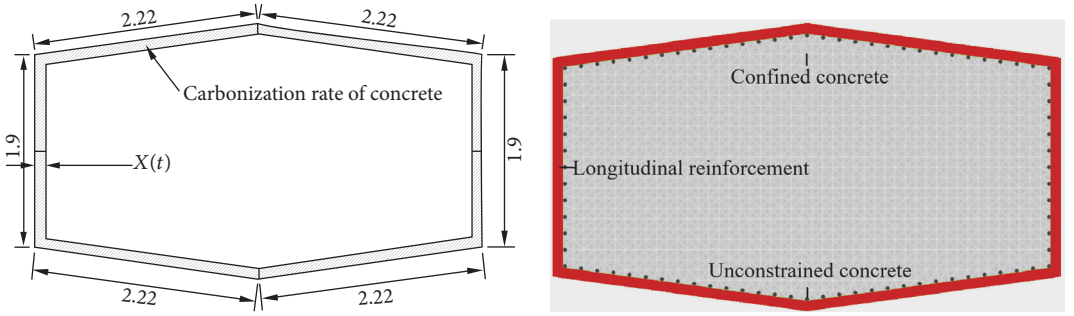

(a) Carbonization rate of concrete (m)

(b) Fiber section of pier

Figure 4: Section of pier.

3.1.2. Definition of Carbonated Concrete. In the study of existing durability of concrete, carbonation depth is used as a parameter, but the effect of its size in structural section cannot be taken into consideration if putting the depth of carbonization as a parameter of carbonization to concrete performance. In this paper, the carbonation rate [28, 29] is chosen as the calculation parameter, as shown in Figure 4, and the calculation of related parameters [30] is shown in (5)-(12). And the peak stress, peak strain, and elastic modulus of concrete in the life cycle are shown in Figures 5–7.

$$x_c = k\sqrt{t} \tag{5}$$

$$k = 3K_{co_2}K_{k1}K_{kt}K_{ks}K_F T^{1/4} RH^{1.5}(1 - RH) \cdot \left(\frac{58}{f_{cuk}} - 0.76\right) \tag{6}$$

$$K_F = 1.0 + 13.34F^{0.3} \tag{7}$$

$$\overline{S} = \frac{A_c}{A} \tag{8}$$

$$\sigma_{cp} = \left(1 + 0.619\overline{S}\right)\sigma_p \tag{9}$$

$$\varepsilon_{cp} = \left(1 - 0.106\overline{S}\right)\varepsilon_p \tag{10}$$

$$\varepsilon_{cu} = \left(1 - 0.459\overline{S}\right)\varepsilon_u \tag{11}$$

$$E_c = \left(1 + 0.503\overline{S}\right)E \tag{12}$$

In the formulas, x_c (mm), t and k (mm/$\sqrt{t}$) are the depth, time and coefficient of concrete carbonization respectively. K_{CO2} is the influence coefficient for concentration of CO_2, K_1 is the influence coefficient of carbonization position, K_{kt} is the influence coefficient of concrete pouring and maintenance, K_{ks} is the influence coefficient for working stress, K_F is the substitution coefficient of flyash, T (°C) is the temperature of concrete, RH is the environmental relative humidity, f_{cuk} (MPa) is the compressive strength of concrete cube, F is the weight ratio of flyash, $\overline{S}$ is carbonization rate, A_c (m^2) is the carbonization area and A (m^2) is total area of cross section, σ_{cp}, ε_{cp}, ε_{cu}, and E_c are peak stress, peak strain, limit strain, and elastic modulus of carbonated concrete, respectively, also

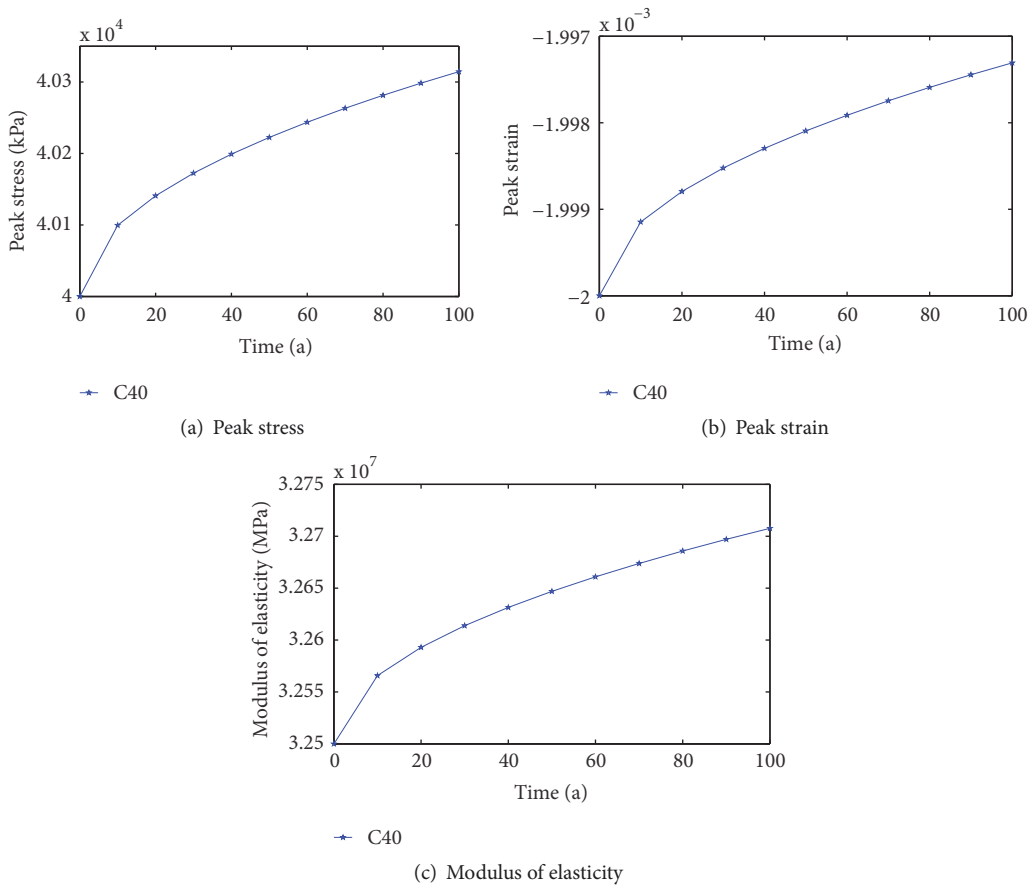

Figure 5: Mechanical property of C40 concrete.

σ_p, ε_p, ε_u, and E are peak stress, peak strain, limit strain, and elastic modulus of the initial concrete, and μ is poisson ratio.

As shown in Figures 5–7, we can know that with the increase of service time, the peak stress increases to a certain extent and varies greatly; the elastic modulus increases slightly; and the peak strain decreases slightly for both the C50 and C40 concrete, after carbonization. In addition, as the mechanical properties of C50 concrete become better, the rate of carbonization of C40 concrete is higher than that of C50 concrete.

3.2. Constitutive Relations and Mechanical Properties of Reinforcing Steel Bars

3.2.1. Constitutive Relation of Reinforcement. The types of longitudinal stirrups and stirrups are *HRB*335 and *R*235, whose diameters are 32 mm and 16 mm, and the thickness of protective layer is 0.09 m. In addition, the location and number of longitudinal reinforcements are shown in Figure 4 and for 1# pier, and the spacing of stirrups in the range of 7 cm - 157 cm, 157 cm - 757 cm, and 757 cm - 968 cm from pier top and 120 cm downward from pier bottom are 10 cm, 20 cm, 10 cm, and 40 cm, respectively; for 4# pier, the spacing of stirrups in the range of 7 cm - 157 cm, 157 cm - 697 cm, and 697 cm - 917 cm from pier top and 120 cm downward from pier bottom are 10 cm, 20 cm, 10 cm, and 40 cm, respectively; for 5# pier, the spacing of stirrups in the range of 7 cm - 157 cm, 157 cm - 1437 cm, and 1437 cm - 1655 cm from pier top and 120 cm downward from pier bottom are 10 cm, 20 cm, 10 cm, and 40 cm, respectively; for 2# pier, the spacing of stirrups in the range of 7 cm - 157 cm, 157 cm - 3437 cm, and 3437 cm - 3644 cm from pier top and 120 cm downward from pier bottom are 10 cm, 20 cm, 10 cm, and 40 cm, respectively; as for 3# pier, the spacing of stirrups in the range of 7 cm - 157 cm, 157 cm - 3297 cm, and 3297 cm - 3507 cm from pier top and 120 cm downward from pier bottom are 10 cm, 20 cm, 10 cm, and 40 cm, respectively.

The constitutive relation model of reinforcement adopts the double line reinforcement model-the Steel 01 model as shown in Figure 8. On the basis of the corrected Giuffré-Menegotto-Pinto reinforcement model, the model can consider the two way Bauschinger effect and isotropic enhancement effect. The parameter values of steel material model are shown in Table 1.

3.2.2. Corrosion Time and Mechanical Properties of Reinforcing Steel Bar. The atmospheric environment in the offshore area belongs to one of the infiltration types chlorine salt eroded environment. Assessment standard for durability of concrete structures (*CECS*220:2007) gives the estimation formula of

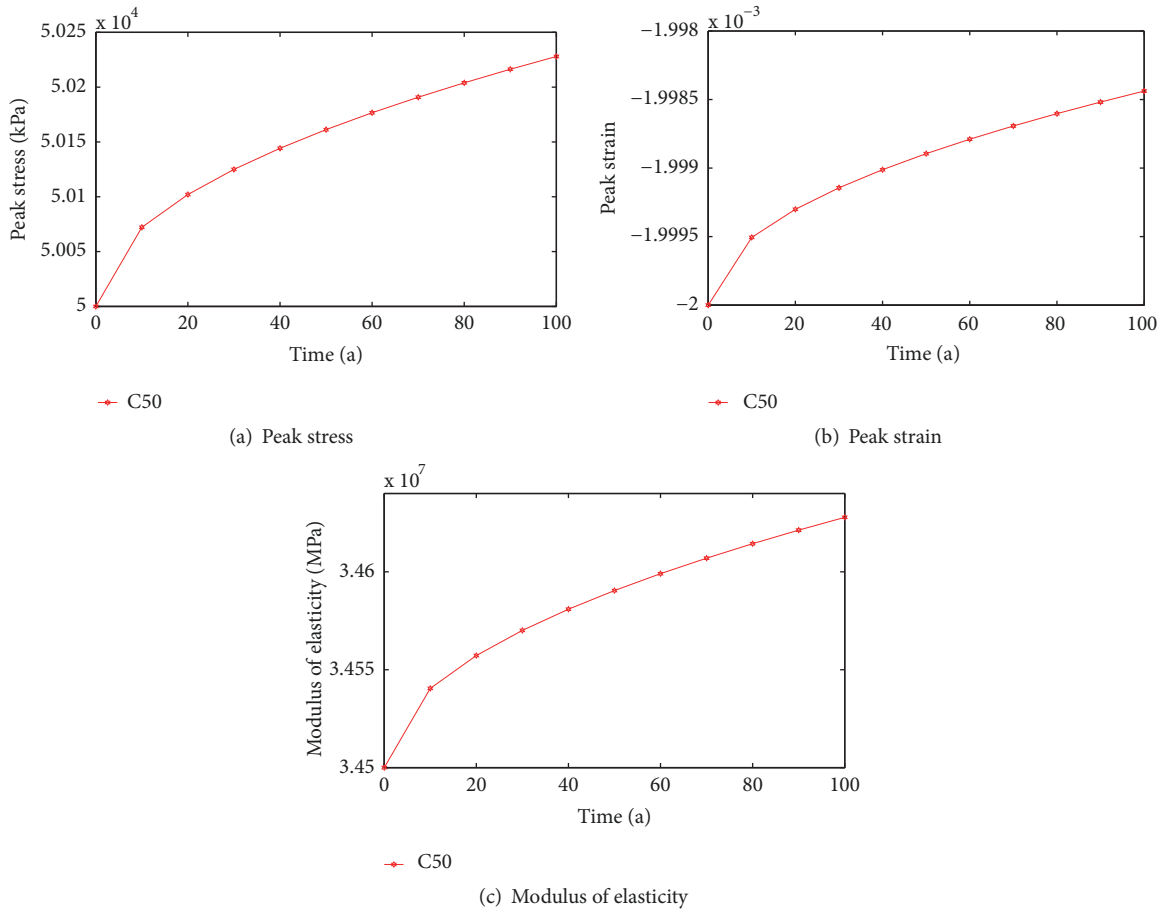

(a) Peak stress

(b) Peak strain

(c) Modulus of elasticity

Figure 6: Mechanical property of C50 concrete.

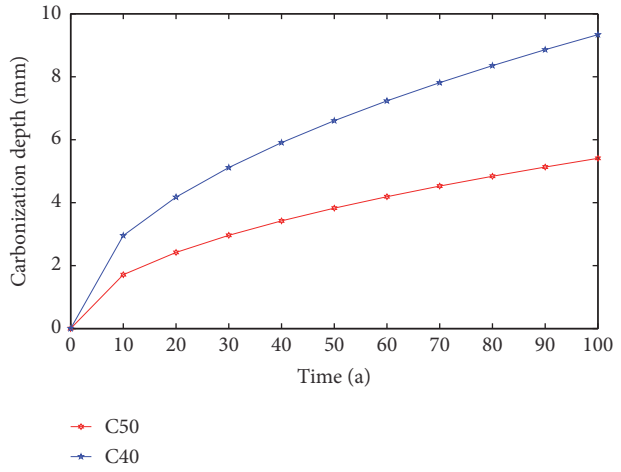

Figure 7: Carbonation rate of concrete.

Table 1: Material parameters of Steel.

Parameter	Modulus of elasticity E_s (MPa)	Yield strength f_y (MPa)	Strain hardening coefficient b
*HRB*335	200000	335	0.01
*R*235	210000	235	0.01

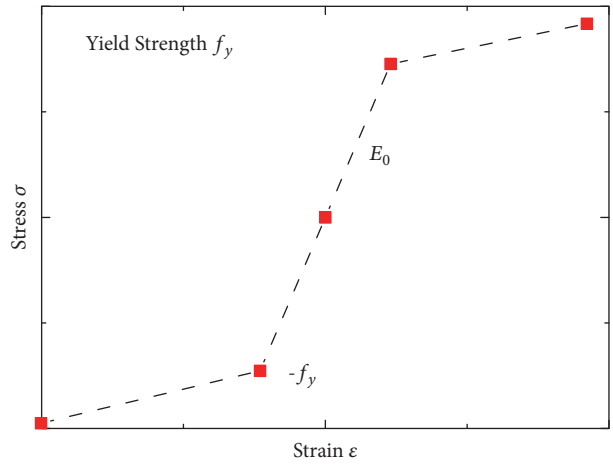

Figure 8: Bilinear reinforcement model of reinforcing steel bar.

Table 2: Chloride ion concentration M'_s on the concrete surface and 0.1km from the coast.

f_{cuk} (MPa)	40	30	25	20
M'_s (kg/m^3)	3.2	4.0	4.6	5.2

Table 3: Chloride concentration correction factor k' on the surface.

The distance from the coast (km)	Near the coastline	0.1	0.25	0.5	1.0
Coefficient of correction	1.96	1.0	0.66	0.44	0.33

Table 4: Initial time of steel-bar corrosion.

Type of concrete	Type of reinforcing steel bar	c (mm)	t_1 (a)	t'_1 (a)	t_i (a)	t_c (a)
$C50$	Stirrup	90	12.5	13.03	15.53	25.66
	Longitudinal reinforcement	106		19.27	21.77	30.39
$C40$	Stirrup	90		11.21	13.71	23.32
	Longitudinal reinforcement	106		16.58	19.08	27.10

the initial corrosion time, the corrosion expansion time, and the corrosion rate of reinforcing steel bar in the corrosive environment. The initial corrosion time of reinforcing steel bar t_i can be estimated by

$$t_i = t'_i + 0.2t_1 \tag{13}$$

In the formula, t_i is the accumulation time of the chloride ion concentration on the concrete surface to reach the stable value; the initial corrosion time of reinforcing steel bar can be estimated by (14) when the time dependence of the chloride diffusion coefficient is not taken into consideration [31, 32]:

$$t'_i = \left(\frac{c}{k}\right)^2 \times 10^{-6} \tag{14}$$

In the formula, c is the thickness of concrete cover (mm); k is Chloride Erosion coefficient which is calculated according to

$$k = 2\sqrt{D}\,\mathrm{erf}^{-1}\left(1 - \frac{M_{cr}}{M_s}\right) \tag{15}$$

In the formula, D is the chloride diffusion coefficient (m^2/a); erf is the error function; M_{cr} is the critical chloride ion concentration for steel corrosion (kg/m^3); M_s is the chloride ion concentration on the surface of the concrete (kg/m^3) which is calculated by

$$M_s = M'_s \cdot k' \tag{16}$$

In the formula, M'_s is the chloride concentration (kg/m^3) on the concrete surface and 0.1km from the coastline which can be selected according to Table 2; k' is the correction factor which can be selected according to Table 3. The calculation results of the initial corrosion time of the reinforcing steel bar in the $C40$ and $C50$ concrete bridge piers in the offshore atmosphere are shown in Table 4, according to the environmental conditions of the bridge site.

The correlated calculation of material properties of reinforcing steel bars (longitudinal reinforcement and stirrup)

after chloride ion corrosion in its life cycle are shown in

$$t_{cr} = t_i + t_c \tag{17}$$

$$t_c = \frac{\delta_{cr}}{\lambda_{cl}} \tag{18}$$

$$\delta_{cr} = \frac{0.012c}{d} + 0.00084 f_{cuk} + 0.018 \tag{19}$$

$$\lambda_{cl} = 11.6 \times i \times 10^{-3} \tag{20}$$

$$\ln i = 8.617 + 0.618 \ln M_{sl} - \frac{3034}{T + 273} - 5 \times 10^{-3} \rho + \ln m_{cl} \tag{21}$$

$$M_{sl} = M_{s0} + \left(M_s - M_{s0}\right)\left[1 - \operatorname{erf}\left(\frac{c \times 10^{-3}}{2\sqrt{Dt_{cr}}}\right)\right] \tag{22}$$

$$\rho = k_\rho \left(1.8 - {M_{cl}}^{\mu}\right) + 10\left(RH - 1\right)^2 + 4 \tag{23}$$

$$\lambda_{cll} = \left(4.5 - 26\lambda_{cl}\right) \cdot \lambda_{cl} \tag{24}$$

$$f_{yc} = \left(1 - 0.339\rho\right) f_y \tag{25}$$

$$E_{sc} = \left(1 - 1.166\rho\right) E_s \tag{26}$$

In the formulas, t_{cr} is rust expansion and cracking time of concrete cover, t_c is the time from corrosion of reinforcing steel bars to expansion and cracking of protective coat, δ_{cr} (mm) is critical corrosion depth of reinforcement bars when the protective layer cracks, c (mm) is thickness of protective layer, d (mm) is diameter of reinforcing steel bar, f_{cuk} (MPa) is compressive strength of concrete, λ_{cl} is average annual corrosion rate of reinforcement bars before cracking of protective layer, i (μA/cm^2) is corrosion current density of reinforcement bars, m_{cl} is local environmental coefficient, T ($^\circ$C) is temperature of reinforcement bar, M_{sl} (kg/m^3) is chloride ion concentration on reinforcing steel bar surface, ρ (KΩ·cm) is resistivity of concrete, M_{so} (kg/m^3) is chloride ion content in concrete preparation, k_ρ is coefficient, ${M_{cl}}^{\mu}$ (kg/m^3) is average chloride ion concentration in concrete protective layer, λ_{cll} is average corrosion rate of reinforcement bar after corrosion expansion and cracking of protective layer, when $\lambda_{cll} < \lambda_{cl}$, $\lambda_{cll} = 1.8\ \lambda_{cl}$, f_{yc} and E_{sc} are the yield strength and modulus of elasticity after carbonization, and f_y and E_s are the yield strength and modulus of elasticity for initial concrete.

According to (17)-(26), we can know corrosion rate, diameter, modulus of elasticity and yield strength of longitudinal reinforcement and stirrup for C40 and C50 concrete, in order to save space, we only give the pictures of diameter and modulus of elasticity, as shown in Figures 9 and 10.

From (13)-(22) and Figures 9 and 10, it can be seen that corrosion of stirrups in concrete occurs earlier than longitudinal reinforcements, because stirrups are close to the concrete surface and they are more susceptible to chloride ions. In addition, the diameter, yield strength, and elastic modulus of longitudinal reinforcement and stirrup in C50 and C40 concrete both decrease with the increase of service time.

In order to simplify the calculation, the corrosion cracking time of the protective layer is taken as the critical life of the concrete failure of the protective layer [33, 34]. Therefore, the effect of concrete protection layer on bridge pier is no longer considered from the bridge full life cycle of 30.39 years when the seismic fragility analysis is carried out for example bridges.

4. Analysis on Damage Index

4.1. Analysis on Damage Index of Bridge Pier. In this paper, the relative displacement ductility ratio corresponding to the failure state of the pier is selected as the damage index of the pier, which can be expressed as $\mu_d = \Delta/\Delta_{cy1}$, μ_d is the relative displacement ductility ratio of the pier, Δ is the maximum relative displacement of pier top in seismic response analysis of piers, and Δ_{cy1} is the relative displacement of the pier top of the reinforcing steel bar for the first yield in this formula.

In this paper, the connection between the 2# and 3# piers and the deck in the bridge is the consolidation, which regards the 2# and 3# piers as rigid piers and assumes that the counter bend point is located at the midpoint of the pier when the damage index is calculated. The calculated damage index of each pier is shown in Table 5.

4.2. Analysis on Damage Index of Bearing. Relative displacement of shear strain and displacement ductility are more able to reflect the mechanical properties of the bearing in practical engineering. Generally, the relative displacement is used as the damage index of bearing in the present study, and the bearing damage index is commonly used in existing studies as listed in Table 6. The type of bearing used for example bridge is the spherical bearing resisting to marine atmospheric corrosion that belongs to the movable steel bearing. Therefore, the bearing damage index given by Bryant to analyze the seismic fragility of the bearing is adopted in this paper.

4.3. Analysis on Damage Index of Bridge Platform. There are few studies focusing on the damage state of bridge platform and there is no uniform method to quantify the damage index of bridge platform at present. The establishment of injury indicators proposed by scholars in various countries is shown in Table 7. In this paper, the relative displacement is used as an index to quantify the seismic damage of bridge platform, and the seismic fragility of bridge platform is analyzed by the bridge platform damage index defined by Murzewski [8].

4.4. Damage Index and Uncertainty of Different Bridge Components. The bending moment curvature analysis of bridge piers is carried out by *XTRACT* [35] software to determine the failure state of the bridge's different components and to quantify its damage index. 150 seismic waves are generated by amplitude modulation. The uncertainties of seismic and structural damage indexes are taken into consideration to analyze the damage index S_c and uncertainty β_c in different damage states of each member under a completion state, as shown in Table 8.

Table 5: The defined failure state of the relative.

Number of pier	Height of pier / m	Initial yield curvature of reinforcing steel bar	Equivalent yield curvature	Curvature of ε_c = 0.004	Limit curvature	Axial force / kN
1#	9.68	0.001010	0.001211	0.002175	0.005113	17274.4
2#	36.44	0.001039	0.001250	0.002231	0.005155	24508.5
3#	35.07	0.001038	0.001249	0.002229	0.005153	24326.1
4#	9.17	0.001002	0.001200	0.002158	0.005095	15828.1
5#	16.55	0.001029	0.001235	0.002212	0.005156	20487.6

Table 6: Limit state of bearing.

Quote	J. Zhang [4]	Bryant [5]	Choi [6]	Choi [6]	Zhang Y [7]	Zhang Y [7]
Type of bearing	Rubber bearing	Movable steel bearing	——	Rubber bearing	Polytetrafluoroethylene skateboard bearing	Rubber bearing
Damage index	Shear strain	Displacement (mm)	Displacement (mm)	Displacement (mm)	Displacement (mm)	Ductility of displacement
Completion state	$\gamma < 100\%$	$\Delta < 37$	$\Delta < 0$	$\Delta < 30$	$\Delta < 90$	$\mu < 1$
Minor damage	$100\% \le \gamma < 150\%$	$37 \le \Delta < 104$	$0 \le \Delta < 50$	$30 \le \Delta < 100$	$90 \le \Delta < 150$	$1 \le \mu < 1.5$
Medium damage	$150\% \le \gamma < 200\%$	$104 \le \Delta < 136$	$50 \le \Delta < 100$	$100 \le \Delta < 150$	$150 \le \Delta < 200$	$1.5 \le \mu < 2$
Serious damage	$200\% \le \gamma < 250\%$	$136 \le \Delta < 187$	$100 \le \Delta < 150$	$150 \le \Delta < 255$	$200 \le \Delta < 300$	$2 \le \mu < 2.5$
Complete collapse	$\gamma \ge 250\%$	$\Delta \ge 187$	$\Delta \ge 150$	$\Delta \ge 255$	$\Delta \ge 300$	$\mu \ge 2.5$

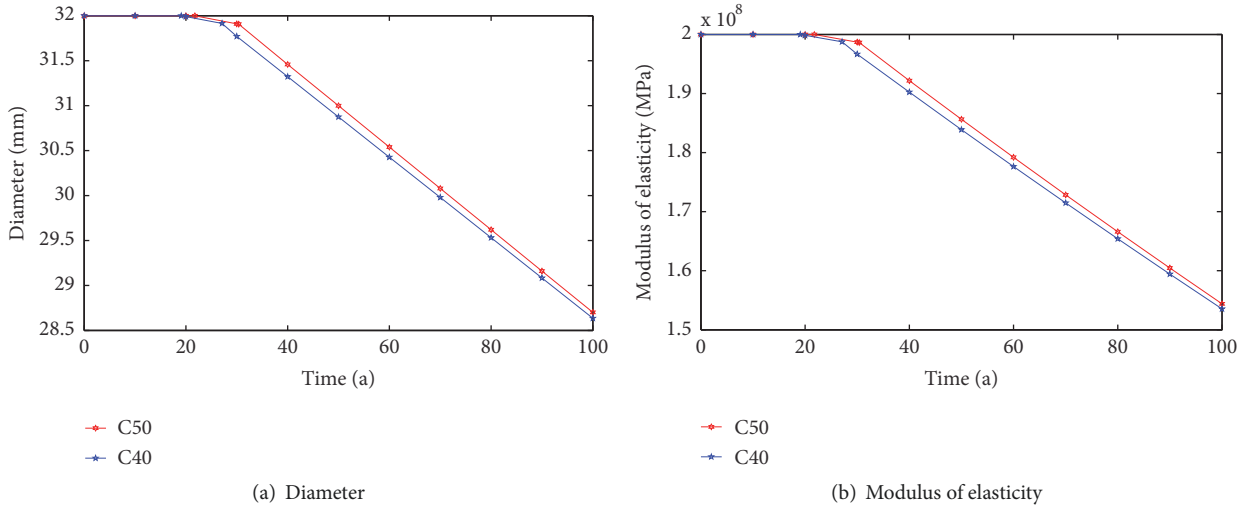

(a) Diameter (b) Modulus of elasticity

Figure 9: Mechanical properties of longitudinal reinforcement.

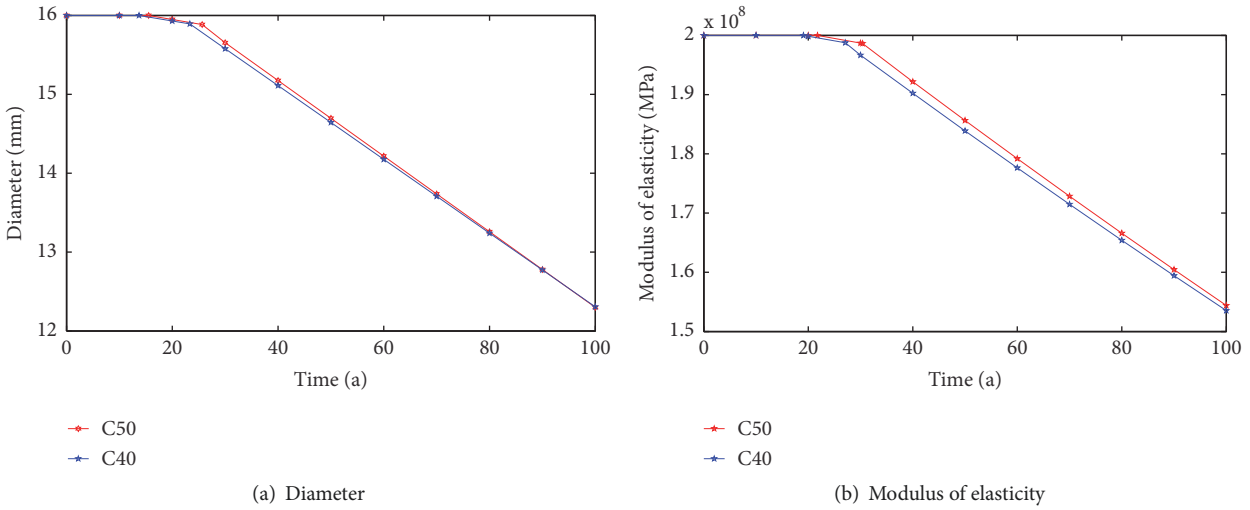

(a) Diameter (b) Modulus of elasticity

Figure 10: Mechanical properties of stirrup.

Table 7: The limit state of bridge platform.

Damage state	Completion state	Minor damage	Medium damage	Serious damage	Complete collapse
Murzewski (mm)[8]	$\Delta < 25$	$25 \le \Delta < 50$	$50 \le \Delta < 100$	$100 \le \Delta < 150$	$\Delta \ge 150$
Bryant (mm) [5]	$\Delta < 37$	$37 \le \Delta < 146$	$\Delta \ge 146$	——	——
Choi (mm) [6]	$\Delta < 4$	$4 \le \Delta < 8$	$8 \le \Delta < 25$	$25 \le \Delta < 50$	$\Delta \ge 50$
Shinozuka (mm) [9]	$\Delta < 30$	$30 \le \Delta < 60$	$60 \le \Delta < 150$	$150 \le \Delta < 300$	$\Delta \ge 300$

Table 8: Damage index and uncertainty of different bridge components.

Components	Minor damage		Medium damage		Serious damage		Complete collapse	
	S_c	β_c	S_c	β_c	S_c	β_c	S_c	β_c
μ of 1# pier	1	0.246	1.199	0.246	1.482	0.472	4.482	0.472
μ of 2# pier	1	0.246	1.203	0.246	1.276	0.472	4.276	0.472
μ of 3# pier	1	0.246	1.203	0.246	1.259	0.472	4.259	0.472
μ of 4# pier	1	0.246	1.198	0.246	1.485	0.472	4.485	0.472
μ of 5# pier	1	0.246	1.200	0.246	1.456	0.472	4.456	0.472
Δ of bearing (mm)	0.037	0.246	0.104	0.246	0.136	0.472	0.187	0.472
Δ of bridge platform (mm)	0.025	0.246	0.050	0.246	0.100	0.472	0.150	0.472

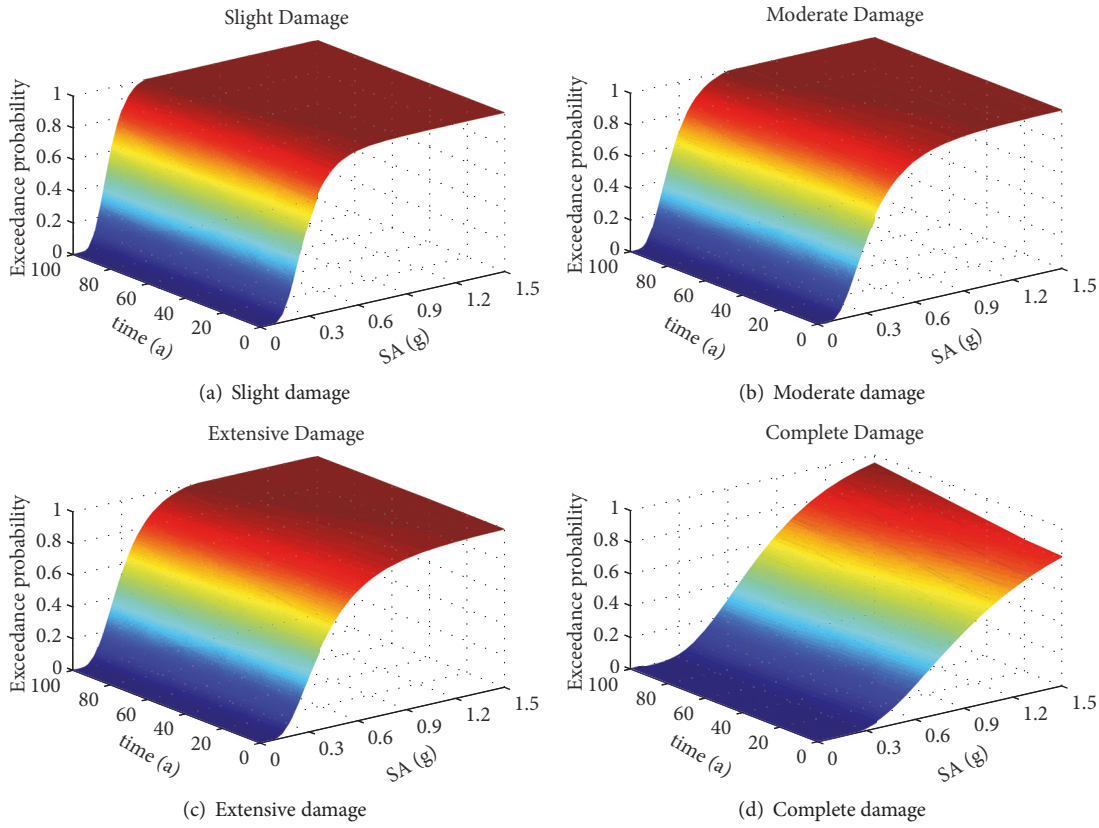

(a) Slight damage (b) Moderate damage

(c) Extensive damage (d) Complete damage

FIGURE 11: The vulnerability surfaces of 1# pier under different damage states.

5. Analysis on Time-Varying Fragility

This paper considers the effect of bridge pier concrete carbonization and steel corrosion on bridge structure dynamic response during service time, in spite of the performance degradation of other components such as deck, bearing, and bridge platform. The time-varying effect of the bridge fragility is introduced by modifying the constitutive relation of concrete and reinforcement in the finite element model of the bridge and the ratio of the confinement strength of the stirrup to the concrete in the core area "*k*."

The key of nonlinear problems lies in the establishment of material nonlinearity and the nonlinear simulation of bridge system in finite element analysis software, that is, the establishment of nonlinear elements. The establishment of material nonlinearity includes the constitutive relationship of concrete and reinforcing steel bar, which have been introduced in Section 3. As for the establishment of nonlinear element, we use "nonlinear Beam Column element" to establish the pier to achieve the nonlinear simulation, and the command is "lement nonlinear Beam Column $eleTag $iNode $jNode $numIntgrPts $secTag $transfTag". And in this command, $eleTag is unique element object tag, and $iNode and $jNode are the start and end node, respectively. $numIntgrPts is the number of Gauss-Lobatto integration points along the element, $secTag is identifier for previously-defined section object, and $transfTag is identifier for previously defined coordinate-transformation (CrdTransf) object.

According to this, we establish the nonlinear finite element model of bridge structure by *OpenSEES* platform, and the seismic fragility curves of components and systems are calculated respectively, for 20, 40, 60, 80, and 100 years by inputting the seismic waves selected for nonlinear dynamic analysis and using the functional formula for seismic fragility as (27) which uses the damage index parameters in Table 8. And the influence of service time on seismic fragility of offshore bridges is also analyzed.

$$p_f = \phi\left(\frac{a + b\ln(IM) - \ln(S_c)}{\sqrt{\beta_c^2 + \beta_d^2}}\right) \tag{27}$$

5.1. Time-Varying Fragility of Pier. In order to describe the seismic fragility of concrete beam bridge in offshore environment during the whole life span more intuitively, this paper compares and analyses the fragility curves of pier during service period, and the seismic variation surfaces of 5 piers under four damage conditions are given, respectively, as shown in Figures 11–15.

It is obtained from Figures 11–15 that in the 100-year service period of the bridge, the seismic fragility of the five piers under the four failure states increases along with the earthquake intensity and the service life of the bridge. The exceeding probability of 1# pier after 100 years' service under the slight damage, medium damage, serious damage, and

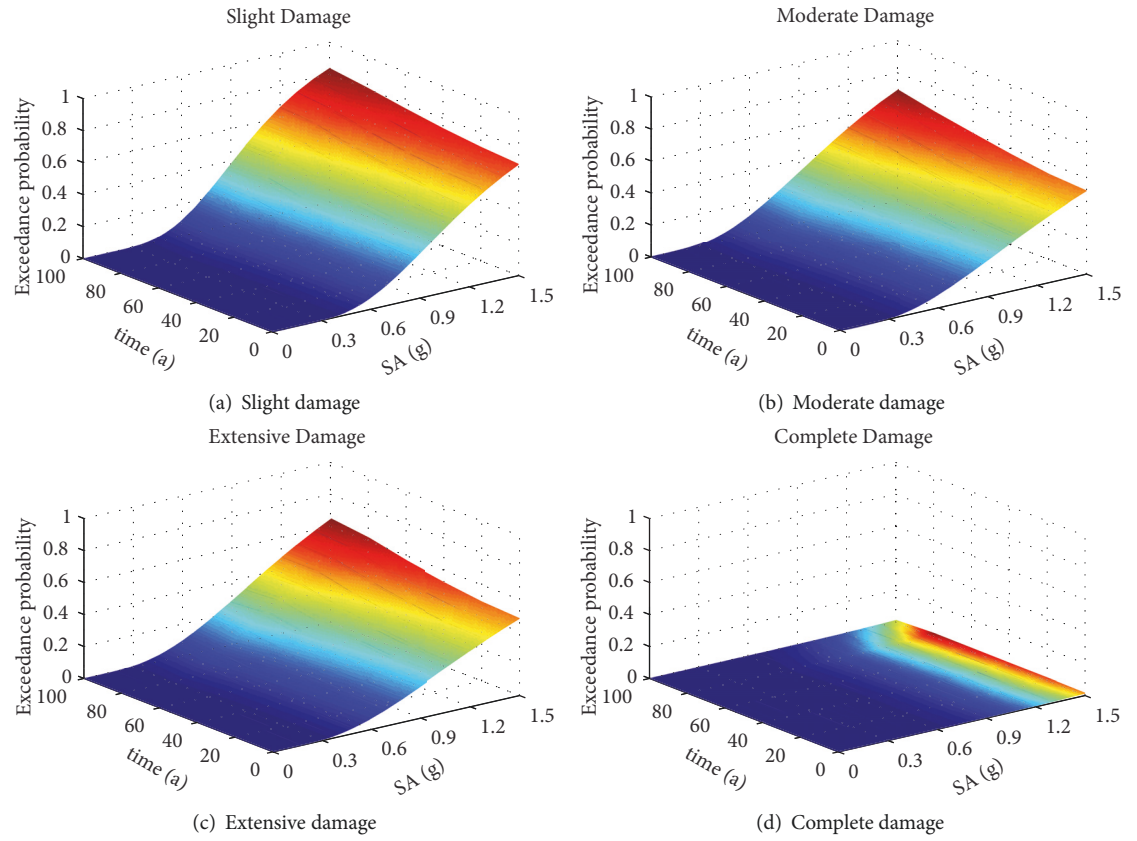

(a) Slight damage (b) Moderate damage

(c) Extensive damage (d) Complete damage

Figure 12: The vulnerability surfaces of 2# pier under different damage states.

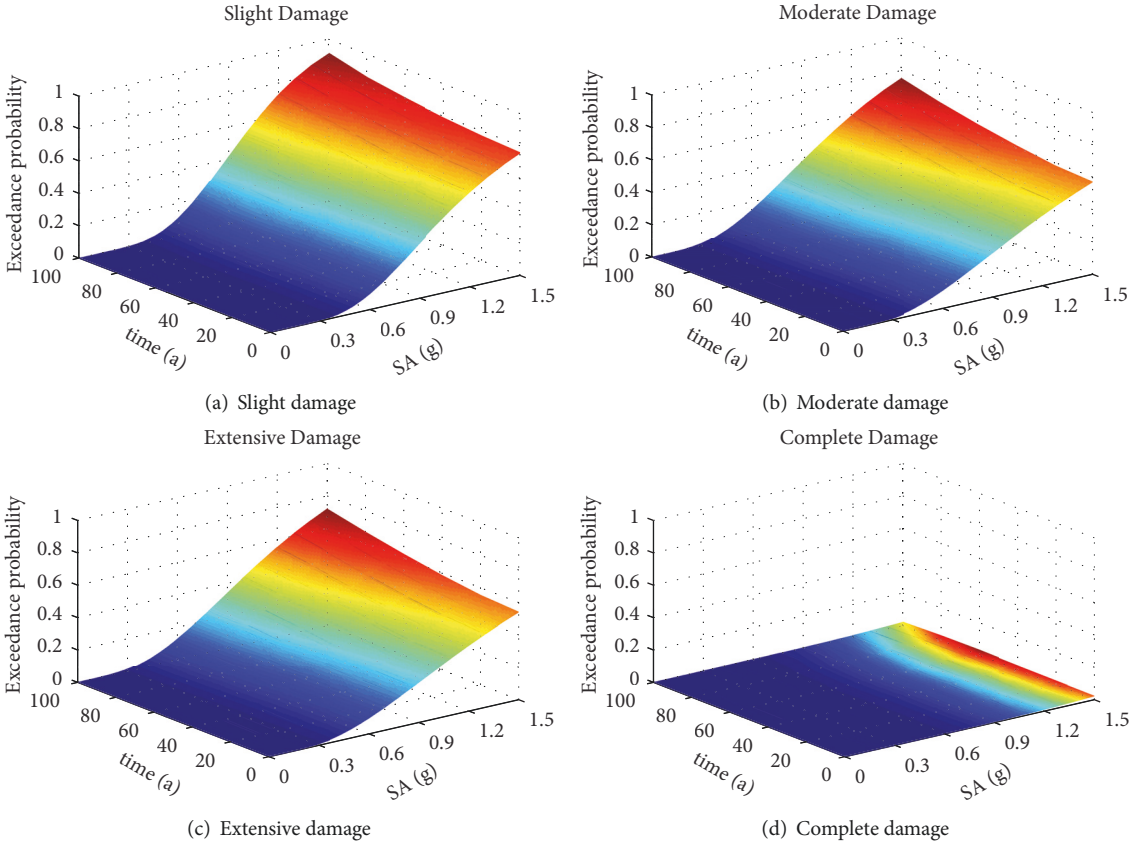

(a) Slight damage (b) Moderate damage

(c) Extensive damage (d) Complete damage

Figure 13: The vulnerability surfaces of 3# pier under different damage states.

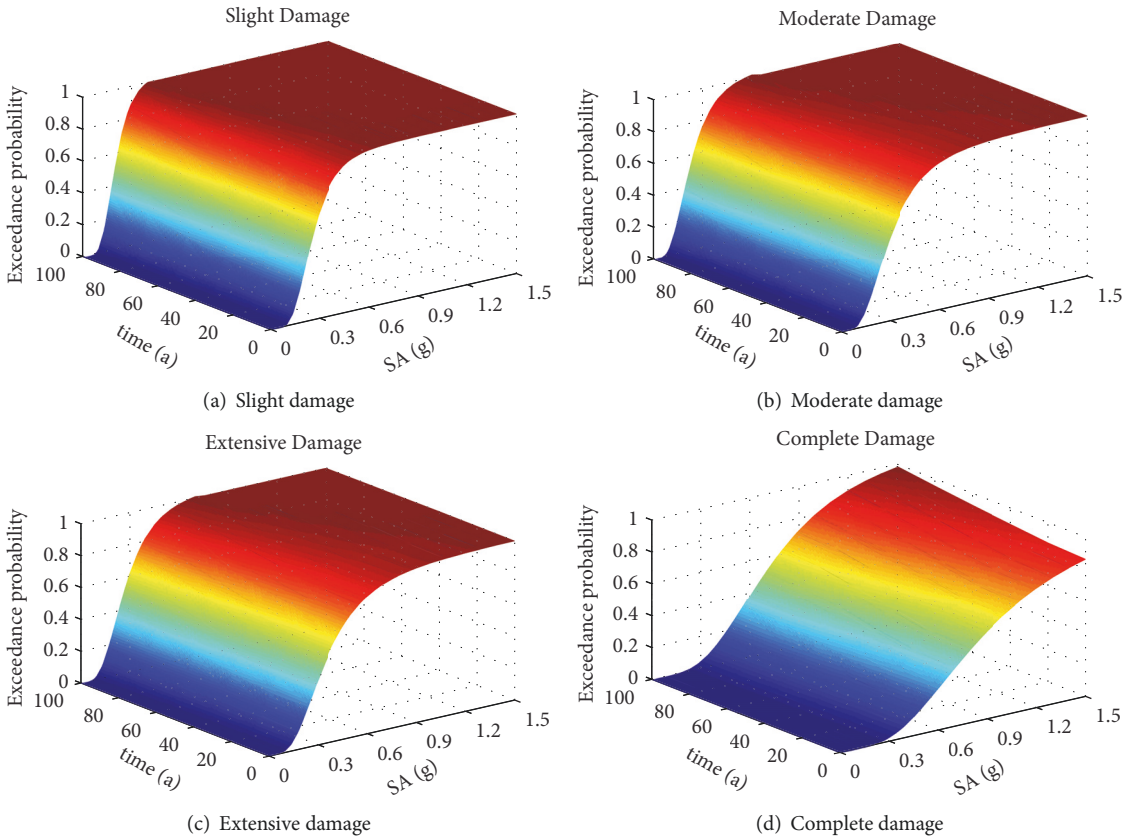

(a) Slight damage (b) Moderate damage

(c) Extensive damage (d) Complete damage

Figure 14: The vulnerability surfaces of 4# pier under different damage states.

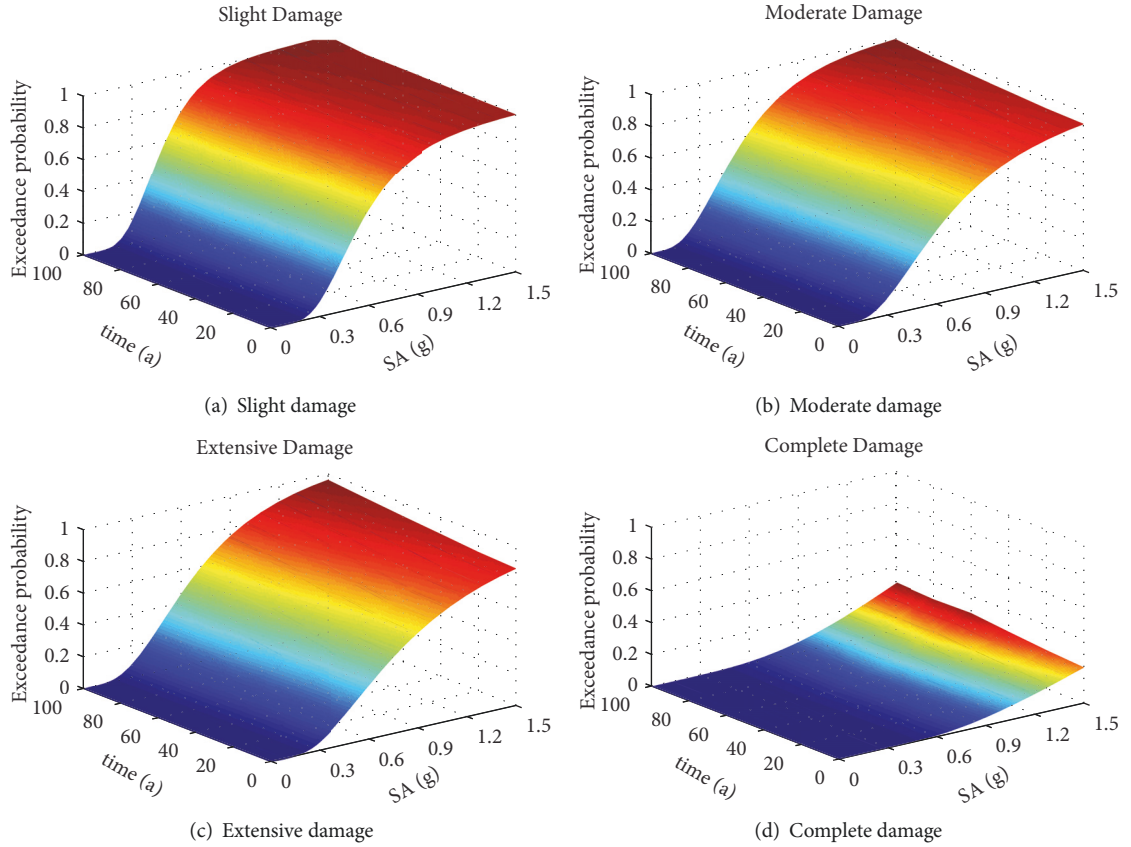

(a) Slight damage (b) Moderate damage

(c) Extensive damage (d) Complete damage

Figure 15: The vulnerability surfaces of 5# pier under different damage states.

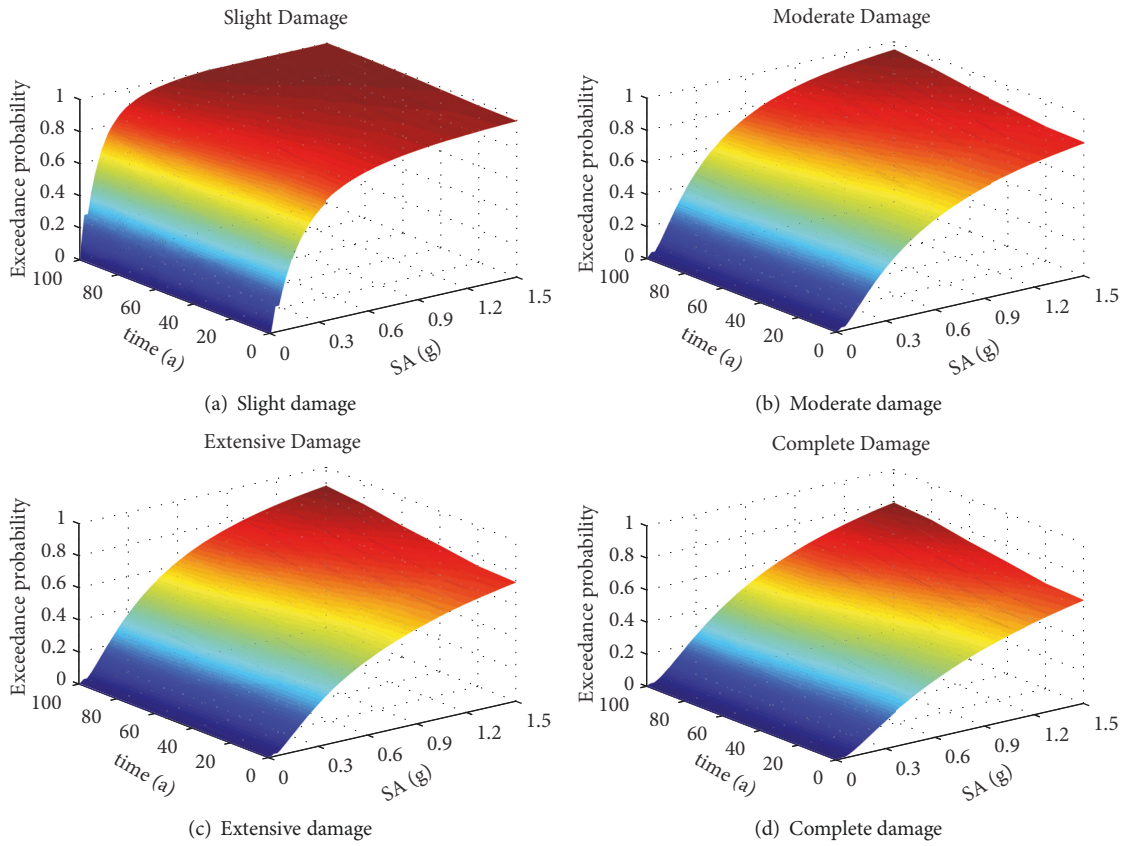

(a) Slight damage (b) Moderate damage

(c) Extensive damage (d) Complete damage

FIGURE 16: The vulnerability surfaces of 1# bearing under different damage states.

the complete collapse can be maximized by 23%, 21%, 20%, and 17%, respectively. Compared with the completion state, the trend of 4# piers is similar to 1# pier. The exceeding probability of 5# pier after 100 years' service under the same conditions can be maximized by 15%, 16%, 15%, and 7%, respectively. Compared with the completion state, the trend of 2# and 3# piers are similar to 5# pier. In the service period, the probability of the 5 piers to surpass all types of damage states is increased with the erosion of chloride ions in the offshore environment and the carbonization of concrete. Seismic fragility of 1# and 4# pier is more susceptible to offshore environment compared with the 2#, 3#, and 5# piers.

With the extension of service time, taking the simply borne pier 1# as an example, the exceeding probability of minor damage to the 1# pier during the 100 years' service period is not less than 97%, the exceeding probability of medium damage is 89%, 90%, 92%, 95%, 98%, and 100%, respectively, the exceeding probability of serious damage is 82%, 82%, 86%, 89%, 93%, and 96%, respectively, and the exceeding probability of complete collapse is 21%, 22%, 25%, 28%, 31%, and 31%, respectively, when SA is 0.6g; the exceeding probability of minor damage of 3# rigid frame pier at service time of 0 and 100 years is 10% and 13%, respectively, the exceeding probability of medium damage is 10% and 15%, respectively, the exceeding probability of serious damage is 9% and 13%, respectively, and the exceeding probability of complete collapse is less than 1%. With the extension of service time, the exceeding probability of all the piers under different failure states increases.

According to the results mentioned above, it is found that the seismic fragility of 1# and 4# bridge piers is more vulnerable to the impact of the offshore environment compared with 2#, 3#, and 5# piers. The exceeding probability of 1#, 4#, and 5# piers under four damage states in the first 20 years is significantly less than that in the latter 80 years for the initial corrosion time of the hoop reinforcement is about 14 years and the initial corrosion time of the longitudinal reinforcement about 19 years, which shows that the mechanical behavior of reinforcement is the main factor to affect the seismic performance of piers. The results show that, for the bridge subjected to chloride ion erosion, the actual seismic capacity of the pier will be continuously decreasing with the extension of the service life, while the seismic demand for earthquake action and the probability to reach ultimate failure state will all be continuously increasing.

5.2. Time-Varying Fragility of Bearing. The degradation of pier's seismic performance is bound to affect the bearing condition under the earthquake action. In this paper, the fragility curves of the bridge bearings in service period are compared and analyzed and the seismic fragility surfaces of five bearings are given as shown in Figures 16–20 so as to analyze the impact of the seismic performance degradation

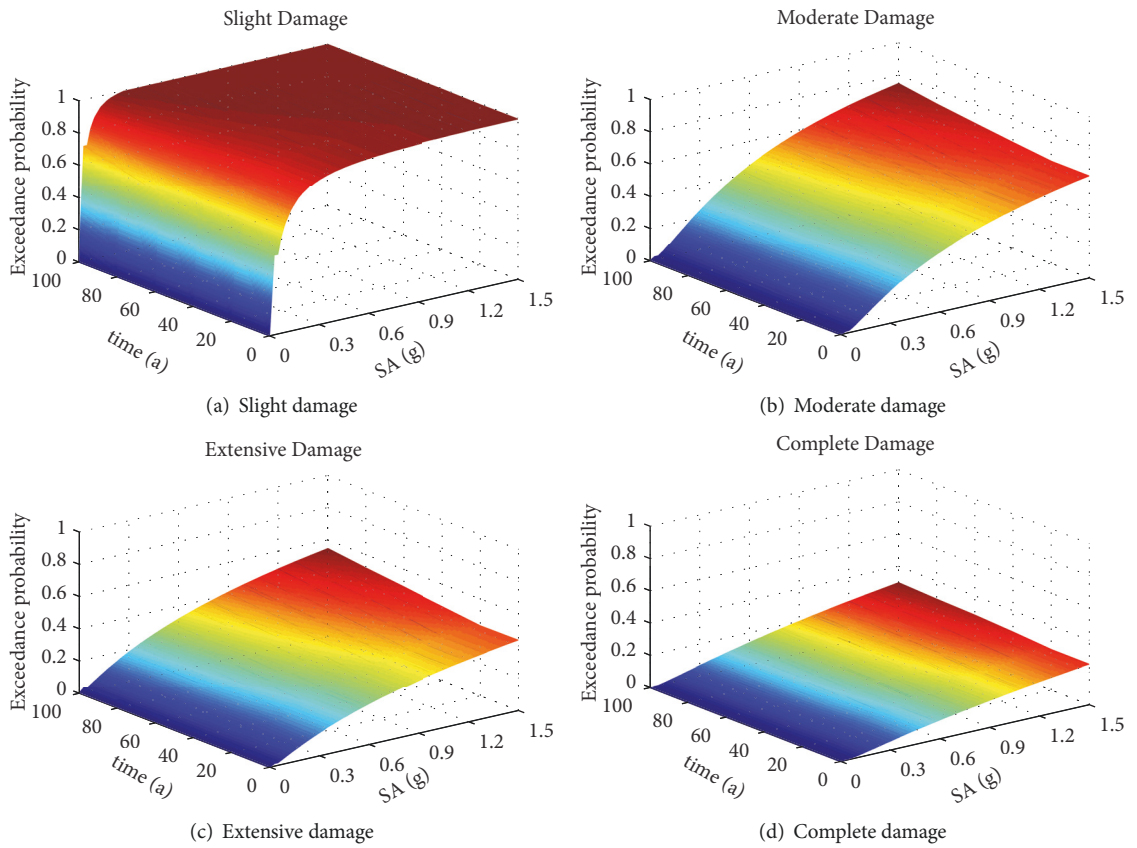

(a) Slight damage (b) Moderate damage

(c) Extensive damage (d) Complete damage

Figure 17: The vulnerability surfaces of 2# bearing under different damage states.

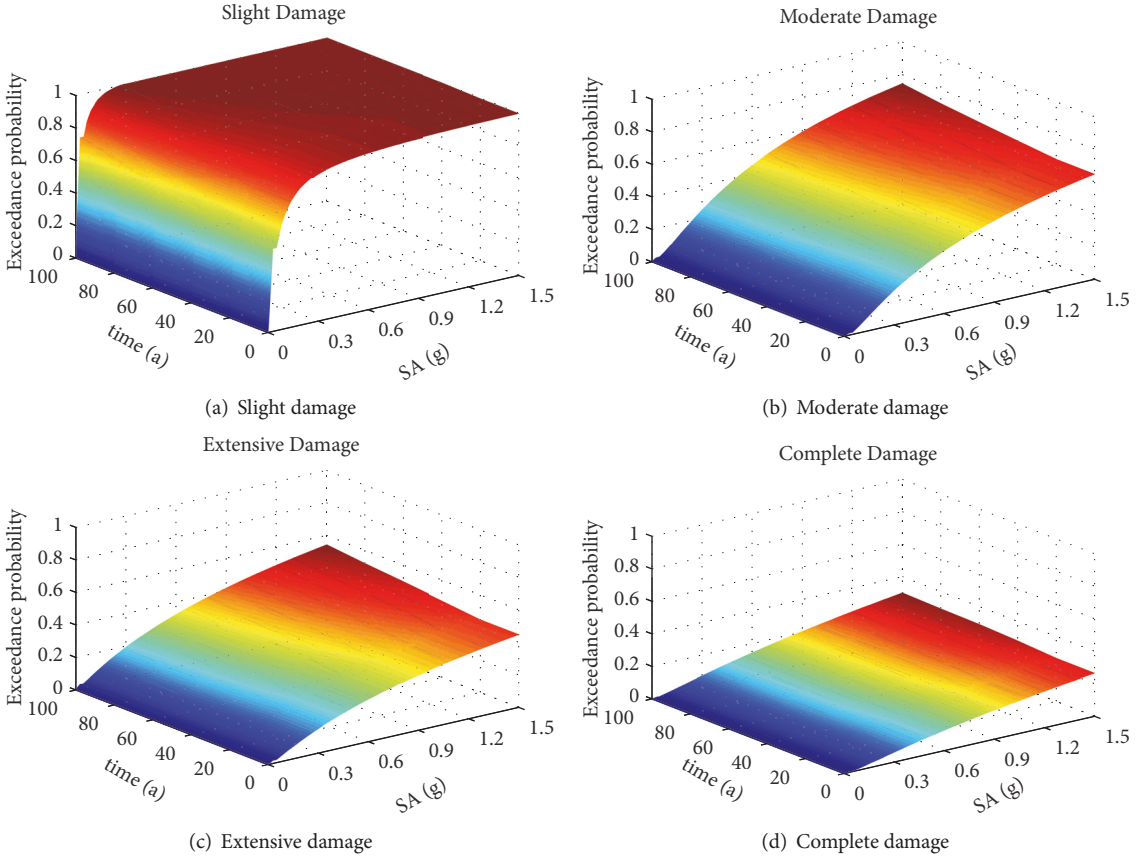

(a) Slight damage (b) Moderate damage

(c) Extensive damage (d) Complete damage

Figure 18: The vulnerability surfaces of 3# bearing under different damage states.

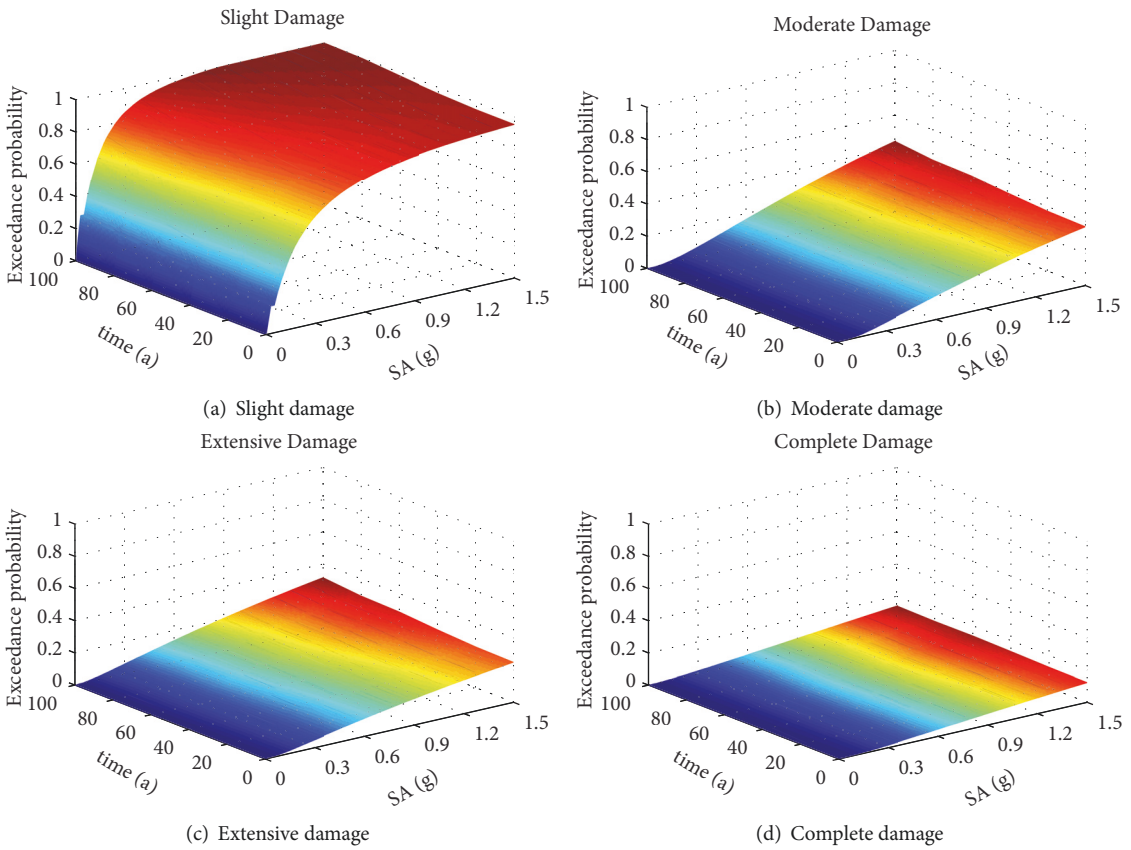

(a) Slight damage (b) Moderate damage

(c) Extensive damage (d) Complete damage

Figure 19: The vulnerability surfaces of 4# bearing under different damage states.

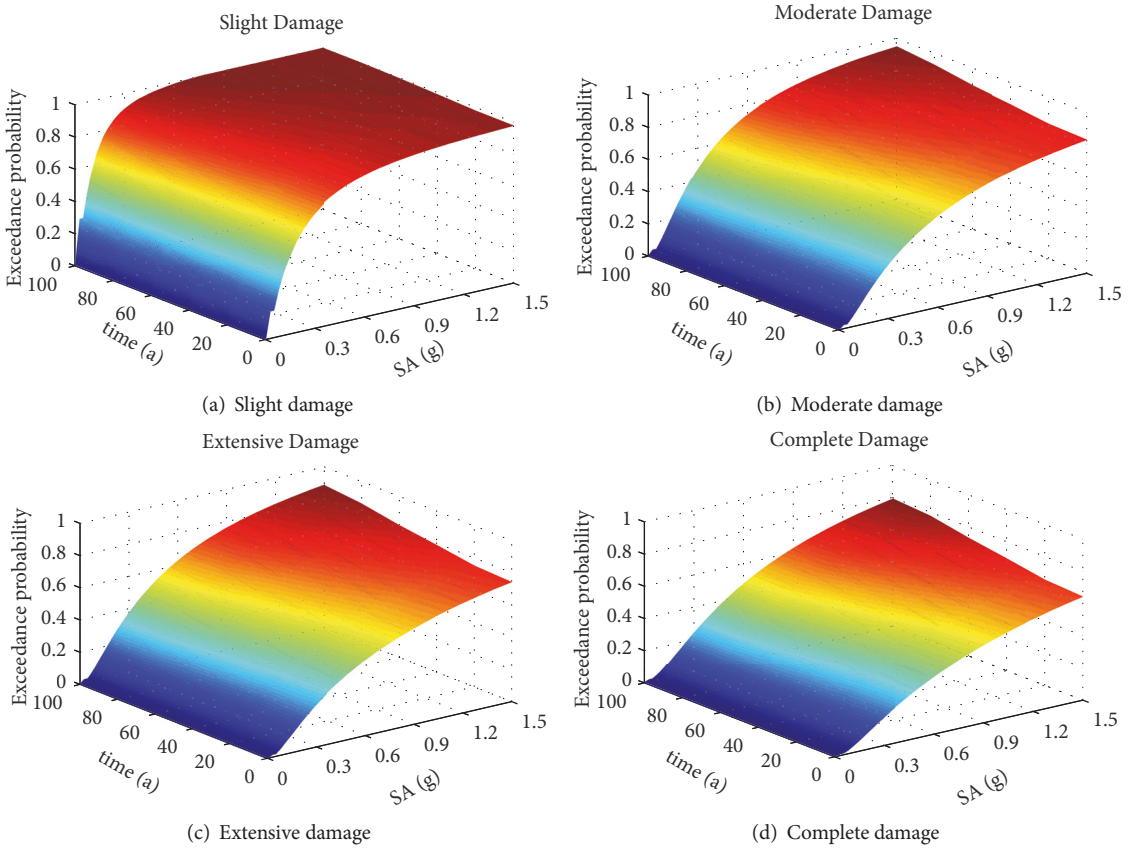

(a) Slight damage (b) Moderate damage

(c) Extensive damage (d) Complete damage

Figure 20: The vulnerability surfaces of 5# bearing under different damage states.

of the pier on the seismic performance of the bearing and to describe the seismic fragility of the bridge bearing in the whole life period directly.

It is obtained from Figures 16–20 that the seismic fragility of five bearings under different damage states is continuously increasing with the increase of the earthquake intensity and service life in the 100-year service period of the bridge. The exceeding probability of $1^{\#}$ and $5^{\#}$ bearings under the minor damage, medium damage, serious damage, and complete collapse can be increased by 22%, 17%, 17%, and 15%, respectively, after 100 years' service compared with the completion state period; the exceeding probability of $4^{\#}$ bearing under four damage states can be increased by 20%, 7%, 7%, and 2%, respectively, after 100 years' service compared with the completion state period; the exceeding probability of $2^{\#}$ bearing under four damage states can be increased by 22%, 12%, 11%, and 5%, respectively, after 100 years' service compared with the completion state period, and the trend of $3^{\#}$ bearing is similar to the $2^{\#}$ bearing's. In the period of service, the probability of five bearings to surpass all kinds of damage states increases with the erosion of chloride ion on the pier, and the seismic fragility increase of the $1^{\#}$ and $5^{\#}$ bearings is the largest. Therefore, we should pay attention to improving the seismic capacity of bearings in the design of offshore bridges.

As the $1^{\#}$ and $5^{\#}$ bearings have the same type and are all located on bridge platforms, their fragility curves are basically the same; similarly, the type of the $2^{\#}$ and $3^{\#}$ bearings and their force mode are the same, and their fragility curves are also basically the same. Therefore, this paper only analyzes the time-varying effects of seismic fragility of $3^{\#}$, $4^{\#}$, and $5^{\#}$ bearings. When *SA* is 0.6g, the exceeding probability of minor damage, medium damage, serious damage, and complete collapse to $5^{\#}$ bearing is 88%, 88%, 91%, 93%, 96%, 99%, 57%, 58%, 62%, 66%, 71%, 74%, 47%, 48%, 52%, 56%, 61%, 63% and 36%, 37%, 40%, 43%, 4 and 7%, in the 100-year service period of the bridge, respectively; as for the $3^{\#}$ bearing in the 100-year service period of the bridge, the exceeding probability of minor damage is not less than 97%, the exceeding probability of medium damage and serious damage is 39%, 39%, 41%, 43%, 44%, 45% and 26%, 26%, 28%, 30%, 31, and 32%, respectively, and the exceeding probability of complete collapse in service time of 10 years and 100 years is 13% and 14%, respectively; for the $4^{\#}$ bearing in the 100-year service period of the bridge, the exceeding probability of minor damage is 83%, 83%, 86%, 89%, 93%, and 97% and the exceeding probability of medium damage, serious damage, and complete collapse in service time of 10 years and 100 years is 15%, 17%, 11%, 14%, and 4%, 5%, respectively.

5.3. Time-Varying Fragility of Bridge Platform. When the displacement between superstructure and pier accumulates to the bridge platform, it will result in a collision between the deck and bridge platform under seismic action. In the present work, the fragility curve of bridge platform during service period is compared and analyzed to describe the change of seismic fragility of bridge platform in the life span of offshore bridges. Taking the left bridge platform as an example, it will show the seismic fragility surface of two bridge platforms, as shown in Figure 21.

As shown in Figure 21, the seismic fragility of the two bridge platforms in each state is continuously increasing with the increase of the earthquake intensity and the service life during the 100-year service period. The exceeding probability of two bridge platforms after 100 years' service under the slight damage, medium damage, serious damage, and complete collapse can be maximized by 33%, 25%, 18%, 13%, respectively, compared with the completion state. The exceeding probability of two bridge platforms under minor and medium damage during the 100 years' service period is no less than 98%, the exceeding probability under serious damage to bridge platform is 70%, 71%, 78%, 84%, 87%, and 87%, respectively, and the exceeding probability of complete collapse is 31%, 33%, 38%, 43%, 44%, and 45%, respectively, when *SA* is 0.6g.

5.4. Time-Varying Fragility of Bridge System. By using seismic fragility of components, the fragility assessment of bridge system will overestimate the seismic capacity of bridges, so it is necessary to combine the fragility of components and the system of the bridge to make an accurate evaluation when the fragility of offshore bridges is assessed during the whole life cycle. The fragility curve of bridge in service period is compared and analyzed to directly evaluate the seismic fragility of offshore bridge during the whole life cycle. The first-order boundary method is used to obtain the upper and lower limit surface of the seismic fragility of the system under four damage states of minor damage, medium damage, serious damage, and complete collapse according to the calculation results of the fragility of the piers, bearings, and bridge platforms, as shown in Figures 22 and 23 and the following:

$$\max_{i=1}^{m}\left[P_i\right] \le P_{sys} \le 1 - \prod_{i-1}^{m}\left[1 - P_i\right] \tag{28}$$

$$\begin{aligned} 1 - \prod_{i-1}^{12}\left[1 - P_i\right] &= 1 \\ &\quad - \left(1 - P_1\right)\left(1 - P_2\right)\left(1 - P_3\right)\ldots\left(1 - P_{11}\right)\left(1 - P_{12}\right) \end{aligned} \tag{29}$$

In the formulas, P_{sys} is failure probability of full bridge system, P_i is failure probability of the component and m is the total number of components; and the Eq. (29) is the formula for calculating the upper limit value of the fragility curve of bridge system.

As shown in Figure 22, the upper and lower limit exceeding probability of the system under the minor damage, medium damage, serious damage and complete collapse can be maximized by 20% and 11% respectively after 100 years' service compared with the completion state period; the upper and lower limit exceeding probability of the system under the medium damage can be maximized by 20% and 23% respectively after 100 years' service compared with the completion state period; the upper and lower limit exceeding

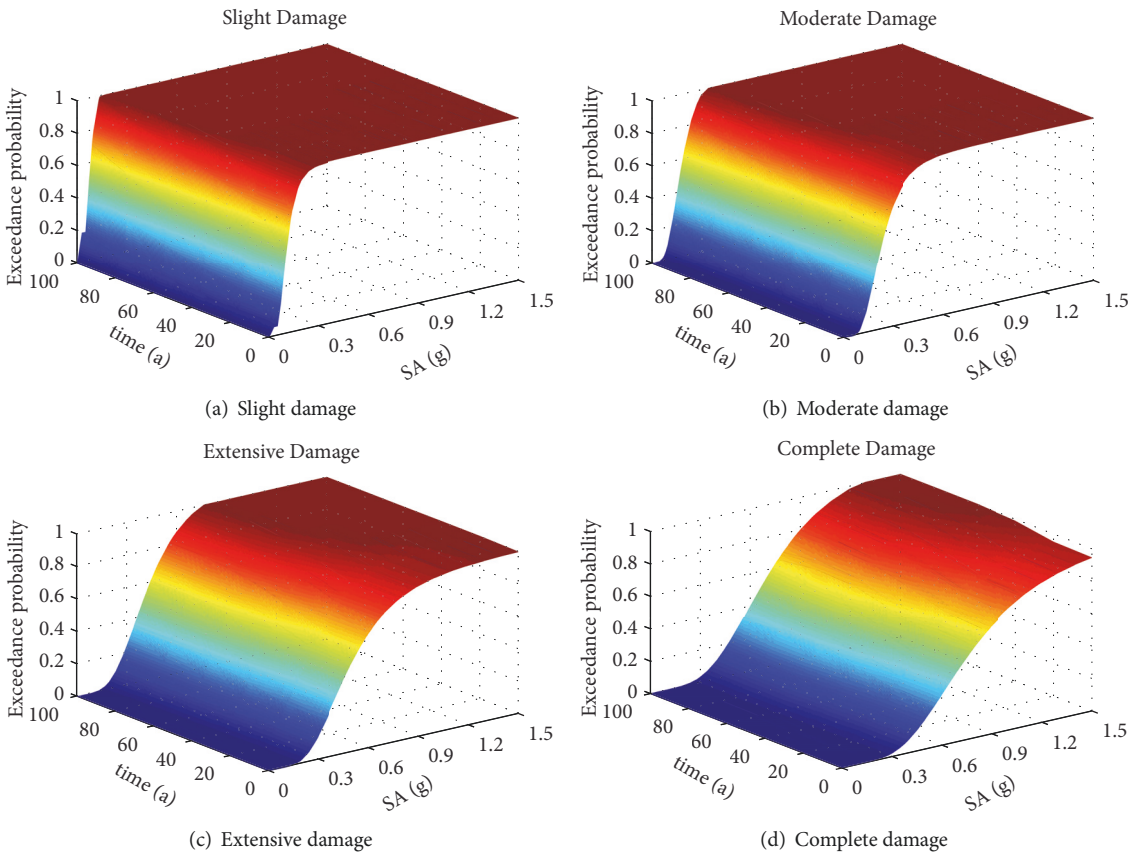

(a) Slight damage (b) Moderate damage

(c) Extensive damage (d) Complete damage

Figure 21: The vulnerability surfaces of left bridge platform under different damage states.

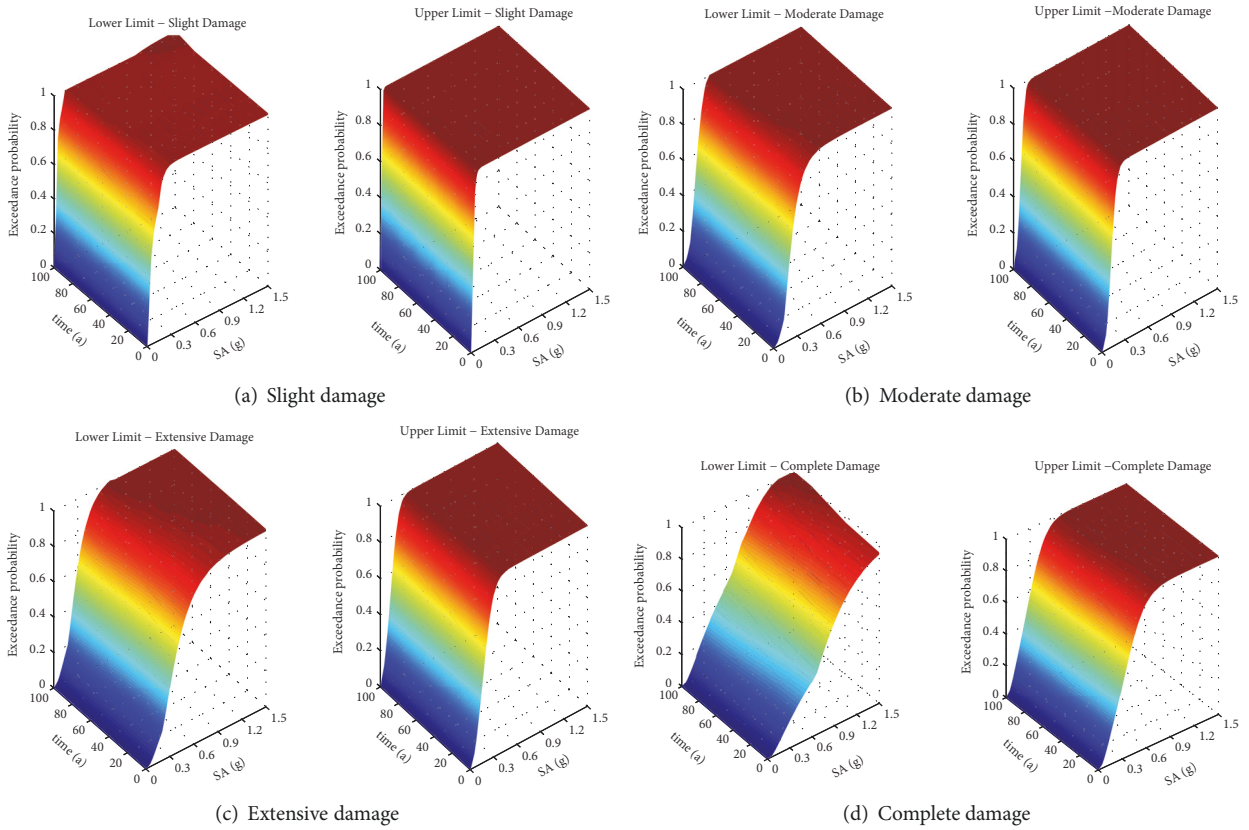

(a) Slight damage (b) Moderate damage

(c) Extensive damage (d) Complete damage

Figure 22: The vulnerability surfaces of bridge system under different conditions.

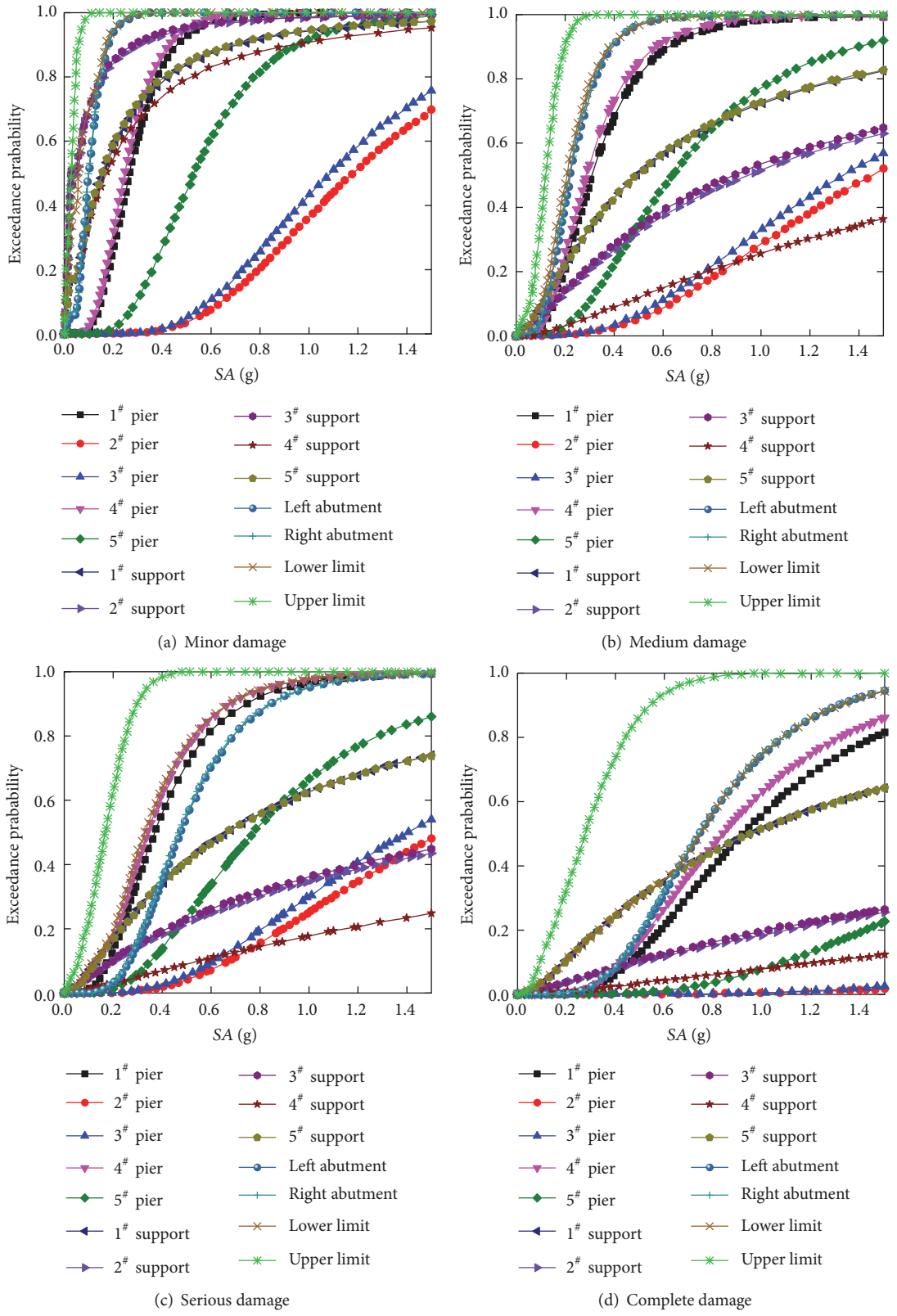

Figure 23: The fragility curves of bridge system and all components under different conditions.

probability of the system under the serious damage can be maximized by 17% and 22% respectively after 100 years' service compared with the completion state period; the upper and lower limit exceeding probability of the system under the complete collapse can be maximized by 12% and 15% respectively after 100 years' service compared with the completion state period. It can be seen that the influence of the offshore environment on the seismic fragility of bridge system cannot be ignored in the service period, in addition, we can know from Figure 23 that the fragility of the system is lower than that of any component, that is to say, the exceeding probability of the bridge system is higher than that of any component. Therefore, the exceeding probability of the system cannot be evaluated by the fragility curve of any component; otherwise, the seismic performance of the bridge system will be overestimated.

The upper and lower limits of the system fragility curve are continuously increasing with the increase of the earthquake intensity and the service life under the four damage states of minor damage, medium damage, serious damage, and complete collapse in the 100-year service period of the bridge. The actual seismic capacity of the bridge members (pier, bearing, and bridge platform) will decrease with the increase of the service life of the bridge, which is mainly influenced by the corrosion of the reinforcing steel bars in the pier and the concrete carbonization on the mechanical properties of the bridge structures.

6. Conclusions

The probability of pier to exceed all kinds of damage states during service period is increasing affected by chloride ion erosion and concrete carbonation in the offshore environment; that is, the actual seismic capacity of the pier will continue to decrease, while the seismic demand for seismic action and the probability to reach the limit state of failure will be continuously increasing.

The seismic fragility of short pier is more susceptible to the offshore environment compared with high piers. The exceeding probability of unconsolidated pier under four kinds of damage states is obviously smaller than that before reinforcement corrosion, which shows that the mechanical behavior of reinforcement is the main factor to affect the seismic performance of piers.

The time dependent seismic fragility curve of the bearing shows that the probability of the five bearings exceeding the various damage states during the service period is increasing. The seismic fragility of bearings at the bridge platform increases the most and is more vulnerable to the offshore environment compared to other bearings. Attention should be paid to improving the aseismic capacity of bearing at the bridge platform in the future design of offshore bridges.

The upper and lower limits of the fragility curve of the bridge system are increasing with the increase of the earthquake intensity and the service life under four damage states of minor damage, medium damage, serious damage, and complete collapse in the 100-year service period of the bridge, and the impact of the offshore environment on the seismic fragility of the bridge system cannot be ignored. It is necessary to make a reasonable evaluation of the seismic fragility of the bridge in the whole life span by combining the fragility of the components and systems.

Data Availability

The data sets used to support the findings of this study are included within the article.

Conflicts of Interest

The authors declare that they have no conflicts of interest.

Acknowledgments

This work was supported by the National Natural Science Foundation of China (Grant nos. 51608488, 51606171, and 51678534).

References

[1] J. Wang, S. Zhou, Z. Zhang, and D. Yurchenko, "High-performance piezoelectric wind energy harvester with Y-shaped attachments," *Energy Conversion and Management*, vol. 181, pp. 645–652, 2019.

[2] S. Zhou and J. Wang, "Dual serial vortex-induced energy harvesting system for enhanced energy harvesting," *AIP Advances*, vol. 8, no. 7, Article ID 075221, 2018.

[3] D.-E. Choe, P. Gardoni, D. Rosowsky, and T. Haukaas, "Seismic fragility estimates for reinforced concrete bridges subject to corrosion," *Structural Safety*, vol. 31, no. 4, pp. 275–283, 2009.

[4] J. Zhang and Y. Huo, "Evaluating effectiveness and optimum design of isolation devices for highway bridges using the fragility function method," *Engineering Structures*, vol. 31, no. 8, pp. 1648–1660, 2009.

[5] G. N. Bryant, *Analytical Fragility Curves for Highway Bridges in Moderate Seismic Zones [Ph.D. thesis]*, Georgia Institute of Technology, 2005.

[6] E. Choi, R. DesRoches, and B. Nielson, "Seismic fragility of typical bridges in moderate seismic zones," *Engineering Structures*, vol. 26, no. 2, pp. 187–199, 2004.

[7] Y. Zhang, Y. Zhang, D. Dias-da-Costa, and D. Dias-da-Costa, "Seismic vulnerability of multi-span continuous girder bridges with steel fibre reinforced concrete columns," *Engineering Structures*, vol. 150, pp. 451–464, 2017.

[8] J. Murzewski, "Probability, Reliability and Statistical Methods in Engineering Design," in *Structural Safety*, A. Halder and S. Mahadevan, Eds., vol. 23, pp. 93–102, John Wiley & Sons, New York, NY, USA, 2001.

[9] M. Shinozuka, M. Q. Feng, J. Lee, and T. Naganuma, "Statistical analysis of fragility curves," *Journal of Engineering Mechanics*, vol. 126, no. 12, pp. 1224–1231, 2000.

[10] D.-E. Choe, P. Gardoni, D. Rosowsky, and T. Haukaas, "Probabilistic capacity models and seismic fragility estimates for RC columns subject to corrosion," *Reliability Engineering & System Safety*, vol. 93, no. 3, pp. 383–393, 2008.

[11] M. Bayat, F. Daneshjoo, and N. Nisticó, "A novel proficient and sufficient intensity measure for probabilistic analysis of skewed

highway bridges," *Structural Engineering and Mechanics*, vol. 55, no. 6, pp. 1177–1202, 2015.

[12] M. Bayat, F. Daneshjoo, and N. Nisticò, "Probabilistic sensitivity analysis of multi-span highway bridges," *Steel and Composite Structures*, vol. 19, no. 1, pp. 237–262, 2015.

[13] J. André, R. Beale, and A. M. Baptista, "New indices of structural robustness and structural fragility," *Structural Engineering and Mechanics*, vol. 56, no. 6, pp. 1063–1093, 2015.

[14] M. R. Salimi and A. Yazdani, "Reliability-based fragility analysis of nonlinear structures under the actions of random earthquake loads," *Structural Engineering and Mechanics*, vol. 66, no. 1, pp. 75–84, 2018.

[15] P. H. Ziehl, M. D. Engelhardt, T. J. Fowler, F. V. Ulloa, R. D. Medlock, and E. Schell, "Design and field evaluation of hybrid FRP/Reinforced concrete superstructure system," *Journal of Bridge Engineering*, vol. 14, no. 5, pp. 309–318, 2009.

[16] M. Khorami, M. Khorami, H. Motahar et al., "Evaluation of the seismic performance of special moment frames using incremental nonlinear dynamic analysis," *Structural Engineering and Mechanics*, vol. 63, no. 2, pp. 259–268, 2017.

[17] J. Ghosh and J. E. Padgett, "Aging considerations in the development of time-dependent seismic fragility curves," *Journal of Structural Engineering*, vol. 136, no. 12, pp. 1497–1511, 2010.

[18] J.-S. Jeon, E. Choi, and M.-H. Noh, "Fragility characteristics of skewed concrete bridges accounting for ground motion directionality," *Structural Engineering and Mechanics*, vol. 63, no. 5, pp. 647–657, 2017.

[19] M. Waseem and E. Spacone, "Fragility curves for the typical multi-span simply supported bridges in northern Pakistan," *Structural Engineering and Mechanics*, vol. 64, no. 2, pp. 213–223, 2017.

[20] J. Simon, J. M. Bracci, and P. Gardoni, "Seismic response and fragility of deteriorated reinforced concrete bridges," *Journal of Structural Engineering*, vol. 136, no. 10, pp. 1273–1281, 2010.

[21] A. Alipour, B. Shafei, and M. Shinozuka, "Performance evaluation of deteriorating highway bridges located in high seismic areas," *Journal of Bridge Engineering*, vol. 16, no. 5, pp. 597–611, 2011.

[22] F. Cui, H. Zhang, M. Ghosn, and Y. Xu, "Seismic fragility analysis of deteriorating RC bridge substructures subject to marine chloride-induced corrosion," *Engineering Structures*, vol. 155, pp. 61–72, 2018.

[23] P. Deng, C. Zhang, S. Pei, and Z. Jin, "Modeling the impact of corrosion on seismic performance of multi-span simply-supported bridges," *Construction and Building Materials*, vol. 185, pp. 193–205, 2018.

[24] Y. S. Chung, "Seismic fragility analysis of RC bridge piers in terms of seismic ductility," *Journal of the Korea Concrete Institute*, vol. 19, no. 1, pp. 91–102, 2007.

[25] A. Toghroli, M. Suhatril, Z. Ibrahim, M. Safa, M. Shariati, and S. Shamshirband, "Potential of soft computing approach for evaluating the factors affecting the capacity of steel–concrete composite beam," *Journal of Intelligent Manufacturing*, pp. 1–9, 2016.

[26] M. Mohammadhassani, M. Suhatril, M. Shariati, and F. Ghanbari, "Ductility and strength assessment of HSC beams with varying of tensile reinforcement ratios," *Structural Engineering and Mechanics*, vol. 48, no. 6, pp. 833–848, 2013.

[27] H.-B. Xie, Y.-F. Wang, J. Gong, M.-H. Liu, and X.-Y. Yang, "Effect of global warming on chloride ion erosion risks for offshore RC bridges in China," *KSCE Journal of Civil Engineering*, vol. 11, pp. 1–7, 2018.

[28] M. Mohammadhassani, S. Akib, M. Shariati, M. Suhatril, and M. M. Arabnejad Khanouki, "An experimental study on the failure modes of high strength concrete beams with particular references to variation of the tensile reinforcement ratio," *Engineering Failure Analysis*, vol. 41, pp. 73–80, 2014.

[29] M. M. A. Khanouki, N. H. Ramli Sulong, M. Shariati, and M. M. Tahir, "Investigation of through beam connection to concrete filled circular steel tube (CFCST) column," *Journal of Constructional Steel Research*, vol. 121, no. 1, pp. 144–162, 2016.

[30] C. D. Atiş, "Accelerated carbonation and testing of concrete made with fly ash," *Construction and Building Materials*, vol. 17, no. 3, pp. 147–152, 2003.

[31] J. Seo and L. P. Rogers, "Comparison of curved prestressed concrete bridge population response between area and spine modeling approaches toward efficient seismic vulnerability analysis," *Engineering Structures*, vol. 150, pp. 176–189, 2017.

[32] Duracrete, "Statistical quantification of the variables in the limit state functions," The European Union - Brite EuRam III - Contract BRPRCT95 - 0132 - Project BE95-1347/R9, 2000.

[33] T. E. Maaddawy and K. Soudki, "A model for prediction of time from corrosion initiation to corrosion cracking," *Cement and Concrete Composites*, vol. 29, no. 3, pp. 168–175, 2007.

[34] R. Zhang, A. Castel, and R. François, "Concrete cover cracking with reinforcement corrosion of RC beam during chloride-induced corrosion process," *Cement and Concrete Research*, vol. 40, no. 3, pp. 415–425, 2010.

[35] R. Fu, K. Liu, G. Men, and L. Hui, "Study on the bearing capacity and influence factors of concrete columns with reinforcing steel bars in core," *Key Engineering Materials*, vol. 723, pp. 731–735, 2017.